論文 / 著書情報
Article / Book Information

題目(和文)	
Title(English)	Human Balance and posture control;Upright stability and feasible movements
著者(和文)	HonarvarMahjoobin Mohammad Hadi
Author(English)	Mohammad Hadi HONARVAR MAHJOOBIN
出典(和文)	学位:博士（学術）, 学位授与機関:東京工業大学, 報告番号:甲第9350号, 授与年月日:2013年9月25日, 学位の種別:課程博士, 審査員:中島 求,井村 順一,早川 朋久,宮崎 祐介,山浦 弘
Citation(English)	Degree:Doctor (Academic), Conferring organization: Tokyo Institute of Technology, Report number:甲第9350号, Conferred date:2013/9/25, Degree Type:Course doctor, Examiner:,,,,
学位種別(和文)	博士論文
Type(English)	Doctoral Thesis

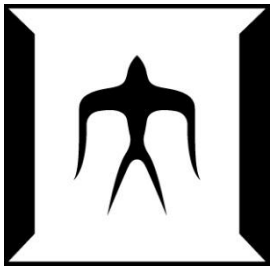

PhD Thesis

Human Balance and posture control; Upright stability and feasible movements

Mohammad Hadi HONARVAR MAHJOOBIN

Under supervision of
Associate Professor Motomu NAKASHIMA

Department of Mechanical and Environmental Informatics
Graduate School of Information Science and Engineering
Tokyo Institute of Technology
Tokyo, Japan
June 2013

Abstract

We humans are bipeds with about two thirds of body mass located on about two thirds of body height above the ground level, so we are an inherently unstable mechanical system, unless a control system is continuously acting. The control of balance, hence, is always a challenge and a side objective in human movements. Any failure in the control of balance may easily lead to an initiation of a fall. The degeneration of the balance control in the elderly and in many pathologies, added to the fact of the increase in our aging population and with increased life expectancy of our elderly, has forced researchers and clinicians to understand more about how the system works and how to quantify its status at any point in time. In this framework two key questions emerge: 1) what is the feasible range of movement for a body to remain balanced while standing, and 2) how good the balance is at a body situation or at every moment during a task.

A feasible region for the control of balance has been proposed previously in the center of mass (CoM) position-velocity plane. This research shows that for a certain individual with given anatomical and mechanical parameters, the feasible movements of the CoM, or more generally the range of states at which the control of balance would be possible, can be analytically found through a mechanical reasoning. This research introduces a subspace of the motion state space, namely the integrated stable subspaces (*ISS*), dependent on the model's anatomical and strength parameters, and proves that the control of balance is possible all over the *ISS*. In order to illustrate how the method may be used in practice, the feasible region for a well-known 2-segment mechanical model as well as for a 3-segment one is found using this approach, and is compared to that found by the conventional method. The feasible region found by this method depends on the physical properties of a body including anatomical parameters of a body as well as the torque (control input) constraints. The method works with any arbitrary shape of the control input constraint.

Regarding question (2), a metric to quantify the level of stability at a body situation (state) is the matter. In this research a new measure for postural upright stability is suggested which assigns a value to a body state addressing how possible the control of balance at that state is. The principle is that a bigger stability value should be granted to a state from which a bigger portion of the society will be able to control their balance and not initiating a fall. Using the population's statistical characteristics and taking advantage of the concept of probability, the postural stability at a state is defined as the probability of the balance to be recoverable over the entire population, and called the *probability of recovery (PoR)*. For a perturbed body state solving the balance recovery problem for a population sample of 600 subjects estimates which portion of them are able to maintain their balance. PoR takes values between zero (0%, no one, low stability) and one (100%, everyone, high stability). It, therefore, describes an attribute of a body state: how possible the control of balance is, or

how safe being at that state is. The PoR calculated for a 3-segment body model is shown for all states on a plane, compared to that found using a 2-segment model, and compared to the conventional metric: the margin of stability (MoS). It is shown, for example, that MoS may be very low at a state from which most of the people will be able to easily control their balance.

The new method of finding the feasible range of movements proposed in this research is, in contrast with the conventional approaches, free of iterative numerical calculations, and hence is very fast. A result is, one may easily change the model parameters and follow how the range of feasible movements will be altered, or study the effect of each anatomical and strength parameter in the feasible range of movements.

The postural upright stability that defined in this research shows how probable avoiding a fall initiation is at a body state. It compares the states directly on the basis of success of the primitive balance control strategies, and hence, is capable to represent the stability at a body state by a single scalar quantifying how good the balance is, or its complementary, how likely the loss of balance is. A corollary, for example, is that a perturbation, no matter of what type or how complicated it is, may be transferred to the state space and replaced with a single scalar: PoR, as a function of the response delay.

Keywords*: balance, perturbation, body state, perturbed state, balanceable region , postural upright stability*

Table of Contents

Chapter 1
Introduction

1.1. The problem of falls

Humans are bipeds and locomote over the ground with two, one, and no foot in contact in standing, walking, and running, respectively. Because of the small support area with respect to the body height, and the fact that about two thirds of our body mass is located on about two thirds of body height above the ground level, we are an inherently unstable mechanical system, unless a control system is continuously acting. The control of balance, hence, is always a challenge and a side objective in human movements. Any failure in the control of balance may easily lead to an initiation of a fall.

Because of the degeneration of the balance control in the elderly and in many pathologies, added to the fact of the increase in our aging population and with increased life expectancy of our elderly, the importance of maintaining mobility is becoming even more critical. It is estimated that one in three persons over the age of 65 is likely to fall at least once each year (World Health Organization [WHO], 2008; Scott, Peck & Kendall, 2004; Tinetti et al., 1994; Tinetti & Speechley, 1989; O'Loughlin et al., 1993). In Canada for example, this translated into approximately 1.4 million seniors who fell at least once in 2005. With the number of older persons in Canada projected to increase from 4.2 million to 9.8 million between 2005 and 2036 (Human Resources and Skills Development Canada [HRSDC], 2010), the estimated number of older persons who will fall at least once in 2036 will increase to 3.3million.

Even more important than the frequency of falling are the consequences of a fall. The fall of an older person can have an enduring and devastating impact. These can be physical or psychological, resulting in injury, chronic pain, a reduced quality of life and, in severe cases, death. Almost half of those who fall experience a minor injury and between 5 and 25 percent suffer from more serious injury, such as a fracture or a sprain (Herman et al., 2006). The hip fracture, which usually implies the fracture of femoral head, is a very common problem for elderly people and can have devastating consequences (cf., Kannus et al. 1999). It is also reported that falls are the leading cause of injury - related hospitalizations and the cause of most hip fractures among seniors, and 20% die within a year of the fracture (Public Health Agency of Canada, 2005). It is also reported in the US that over 2.2 million adults over 65 years old were treated in the emergency room for fall-related injuries in 2009, 20422 of which concluded in death (Centers for Disease Control and Prevention [CDC], 2010). In Europe the situation is similar. As reported by the World Health Organization (World Health Organization [WHO], 2002) the falls as a cause of death dramatically increase with increasing age. For instance, in two countries that could be considered representative of Europe, The Netherlands and Spain, the rate of deaths caused by falls of people aged above 75 level reach values between 30 and 40 deaths per 100000 inhabitants. These values are extremely high, taking into account that they represent only the deaths caused directly from a fall.

In addition, many people limit voluntarily their independent activity due to the fear of falling. Thus, the psychological impact of a fall may result in a post - fall syndrome that includes dependence on others for daily activities, loss of autonomy, confusion, immobilization and depression (World Health Organization [WHO], 2008), which is considered of the most important aspects for a good quality of life (see e.g. Imms & Edholm, 1981).

So, falls are a major health problem in particular for elder adults, and this fact has forced researchers and clinicians to understand more about how the system works and how to quantify its status at any point in time.

1.2. How we regard the problem: The state space framework

In order to reduce consequences and costs associate with falls, three main topics should be addressed, observing the three stages of a fall: perturbation, reaction, and collision, as follows:

1) The perturbation onset to one's balance, aiming in minimizing the incidence of a perturbation in one's balance which will conclude to a reduction of loss of balance occasion, and will directly lead to a reduction in fall incidences. It is related to the environmental factors, gate abnormalities, and the like.
2) Response to a perturbation, trying to control the balance and not initiating a fall, when a perturbation is already happened and the balance is disturbed.
3) Approach to the ground, aiming in minimizing the injuries, when a fall has already been initiated and a collision to the ground is unavoidable.

This research has focused on the second area: the control of balance when it is already perturbed.

If we look at the epidemiology of falls we see reports that about 50% of the falls occur during some form of locomotion (Ashley et al. 1977; Gabell et al., 1985; Overstall et al., 1977; Prudham & Evans, 1981). It is during walking that we challenge our system the most: initiating and terminating gait, turning, avoiding obstacles (altering step length, changing direction, stepping over objects, etc.), bumping into people and objects. However, in spite of the epidemiological evidence that most falls occur during one form of locomotion or another, a large body of research into balance during quiet and perturbed standing has evolved, in order to study the upright balance, its mechanisms and conditions, in general. Thus, much of the research has attempted to perturb the balance system in a large number of ways in order to quantify the human response. When the researcher is interested in reactive responses he/she introduces unexpected perturbations. On the other hand, proactive control will require either voluntarily initiated internal perturbations (such as raising an arm) or anticipatory well-learnt perturbations (such as is experienced many times over the walking cycle). (Winter, 1995-a) An inherent difficulty in such a research theme is that, a large number of perturbations in different types, severities, and complexities must be considered in order to study the human response. In fact, in many studies a (few) particular form of balance perturbation are studied, such as a horizontal

impulse at a certain point in the body height (see e.g. Atkeson & Stephens, 2007), a horizontal movement of the base of support (Le Goic et al. 2012), etc. In such studies it would be difficult to generalize the findings to a generic perturbation in one's balance. In this research we work in a different framework.

Following a perturbation, like a slip, trip, stumble, etc., no matter what the source, type, or complexity of the perturbation is, right after some response delay and exactly when the individual starts its response trying to regain its balance, the body situation can be described by a single point in the body *state* space. We use the term "state" to describe human situation at a moment which is the combination of all postural and movement variables, such as joint angles and angular velocities. It may be expressed mathematically by a vector the components of which are postural and movement variables, e.g. joint angles and all angular velocities. State space is then a virtual n-dimensional space, each axis of which is one of the joint angles or angular velocities. n is the number of state variables. A single point in the state space uniquely describes a body situation in the reality. Any body movement, such as the action of control of balance, may be described uniquely by a curve or trajectory in the state space, showing what the body situation is at every point in time. So, in this study we never use terms like slip, impact, trip, etc. Whatever we say is about the body state a person has at a moment.

1.3. The two key questions

A fall begins with a dynamical perturbation in one's balance, but not every perturbation initiates a fall. The possibility of maintaining stability from at perturbed situation depends on two factors. First, the individual's abilities which shows the range of perturbations or states that is tolerable for a certain individual, and second, the severity of the perturbation which may be interpreted as the subject's state right after the perturbation onset, or after some reaction delay. Thus, studying the control of balance, or equivalently, the risk of loss of balance, may be focused on two sides: 1) the individual side and studying the risk of fall initiation for a certain subject and different situations, and 2) the body state and consider how risky a fall initiation is at a certain body situation (posture & movements) for different individuals. In this framework 2 questions emerge:

1. What is the range of feasible movements for the control of balance? or equivalently, in what region in the state space the control of balance would be possible?

2. How good is the balance at a given body state?

In the first question, for a certain individual with known anatomical and strength parameters the range of movements or body states is to be obtained at which the control of balance would be feasible. Such a range varies with the subject, and is a representative of one's ability in handling balance perturbation. In the second question, a method to quantify the upright stability at a certain stare is the matter, seeking a postural stability metric to assess the upright balance .

1.4. Current answers

A single, quantitative criterion for assessing a person's ability to control balance is often difficult to establish, primarily because there are many feasible movements to choose from which accomplish the same task. One strategy for resolving this issue is to quantify various constraints that a person has to negotiate in the performance of a task, and then to use these constraints to identify the range of feasible movements in which the control of balance can be maintained.

Previous studies have investigated feasible ranges in acceleration, torque, or manual force application spaces under various constraints necessary for a person to maintain standing balance by keeping the feet stationary (Gordon, 1990; Kerk et al., 1994; Kuo, 1995; Kuo and Zajac, 1993; Levine et al., 1983; Nashner et al.; 1989, Yang et al. 1990). For instance, Gordon (1990) introduced the idea that certain physical constraints (i.e. muscle strength, the need for the foot to remain on the floor, etc.) can be mapped into the acceleration space. In his work, a model of the foot segment was used to introduce constraints on the dynamics of a three-joint planar model of standing. A feature lacking in these studies was an understanding of how the range of feasible movements could be influenced by the interaction of several task constraints. For example, the interplay between velocity and position has never been examined in balance dynamics, presumably because velocities are considered low in nearly static standing.

For a long time the feasible movements of a body for the control of balance were described by a single condition related to the position of the body CoM: the horizontal component of the location of the body CoM has to be confined within the base of support (BoS) (Borelli, 1680; Dyson, 1977; Patla et al., 1990; Kuo, 1995). It has been first brought to the attention by prof. Pai and his group that this condition is neither sufficient nor necessary in dynamical situations (Pai & Patton, 1997). The velocity of the center of mass should also be accounted for in describing the feasible movements for the control of balance, since it governs the destiny of the CoM position. Even if the CoM is above to BoS, control of balance may be impossible if the velocity of CoM is large enough and directed outward. The reverse is also possible: even if the vertical projection of the CoM is outside the BoS but its velocity directed towards it, control of balance may be feasible. They defined a "motion state" consisting of two variables: the horizontal component of the location and velocity of the CoM in the sagittal plane. They obtained a region in the corresponding two-dimensional state space and suggested that the condition for the balance to be maintained for a body situation is that its corresponding motion state lies within this feasible region. However, in order to figure out the feasible recovery region they used a numerical searching and optimization method which includes iteratively solving the problem of whether maintaining the balance is possible at initial motion states. It is computationally expensive.

The feasible region has also been obtained in research dealing with the optimal balance recovery trajectory (see e.g. Atkeson & Stephens, 2007). The area in which an optimal trajectory finder has a solution is the feasible region. Trivially the computation burden in this approach is very heavy as well. Another work used a curve fitting method (Yang et al.,

2008) in order to express the boundaries of the feasible region obtained by Pai & Patton (1997) beforehand, which only simplifies working with the feasible region. Hof et al. (2005) simplified the dynamic equation of the same two-segment mechanical model of body and developed a very simple equation for the two main boundaries of the feasible region. In this research as well as those done in Pai & Patton (1997), average muscle strength is assumed, and hence the effect of muscle strength is left out of view since for an average amount of strength the geometric constraints determine the feasible region.

Though in Pai & Patton (1997) additional calculations have been conducted in order to find the threshold values where key parameters (strength, friction, etc.) started to affect the feasible region, there is still no method, whether analytic or a computationally light numerical method, to figure out the feasible recovery region in the state space for any arbitrarily given anatomical and strength parameter values. Such a method will be necessary, for example, to consider the role of each constraint or parameter in altering the person's feasible movement range.

The traditional view to the upright stability at a body situation was expressed as the vertical projection of the center of mass (CoM) has to be within the base of support (BoS) for the balance to be maintained, and its shortest distance to the edge of BoS was used to show how far from the balance a state is (Borelli, 1680; Dyson, 1977; Kuo, 1995; Patla *et al*., 1990, Shumway-Cook, 1995; Winter, 1995-a). BoS is the area which transfers the body weight to the ground, i.e. the possible range of the center of pressure (CoP). Later, it has been brought to attention that this criterion is neither sufficient nor necessary in dynamic situations, and the velocity of the CoM should also be accounted for (Pai & Patton, 1997; Iqbal & Pai, 2000). They obtained a feasible stability region in the position-velocity plane, which was reformulated later by Hof *et al*. (2005) as: the condition for dynamic stability is being the "XcoM" within the BoS. XcoM is the "*position of the extrapolated CoM*" which is a linear combination of the horizontal position of CoM and its time derivative. They also suggested a new measure for stability of a body state, the margin of stability (MoS), as the shortest distance of XcoM to the edge of BoS. However, MoS is not well related to the "possibility" of maintaining the balance or "safety" at a state. It may be very small for a state while it is highly safe. The reverse is also true: high MoS is not necessarily highly stable.

A new metric for upright stability should be developed which directly represents how possible the control of balance at a certain body state is, or how safe being in a state is.

1.5. The objectives of this research

The objective in this research is to develop an analytic method to figure out the range of feasible movements for the control of balance for a given individual with certain anatomical and strength parameters. Such a method will be computationally light, and hence, it would be quite practical to study the role or effect of every physical parameter in the range of feasible movements, by altering a parameter and follow up how the feasible range of movements will be changed. Thus a thorough parametric study on one's ability to handle balance perturbation can be performed efficiently.

A second objective of this research is to develop a new metric to assess the upright balance at a given body state, so that directly bears the concept of stability at a state, or represents the safety for an individual to be at a certain state, with respect of the fall risk.

1.6. Thesis content

In the present text, we first introduce the class of mechanical models our theories may be used on in Chapter 2, as well as two models which we will use as platforms to apply the theories and demonstrate the results.

Chapter 3 introduces the method we propose as an analytic way to figure out the range of feasible movements. It includes definition of the balanceable region, description of the key idea on a very simple mechanical model, then explain the theory and theorems for a more generic model, apply the method on a 2-segment and a 3-segment mechanical model, and a discussion on the method, results, and limitations.

In Chapter 4 the new metric we suggest to assess the postural upright stability will be described. The so called no-risk curve will be introduced and obtained first, and then the new metric for upright balance called PoR will be introduced conceptually, then it will be described that how PoR can be calculated for a body state, and the method will be applied again on 2 mechanical models to find the PoR. Results will be discussed and main limitations of this method will be introduced.

Chapter 5 presents a conclusion for the presently reported work, and brings some suggestions for future extensions.

Chapter 2
Mechanical Model

2.1. Introduction

Studies of human standing balance have revealed several strategies to compensate for perturbations: the *ankle strategy,* in which torque about the ankle joints is used to balance and the rest of the body is held in a fixed posture, the *hip strategy,* in which torque about the hip joints is used to generate horizontal ground forces moving the center of mass, the *squat strategy,* in which the knees and hips are flexed to lower the center of mass (Runge et al., 1999; Hemami et al., 2006), and the *step strategy,* in which a step is taken (Nashner et al., 1985; Horak & Nashner, 1986). These multiple strategies reflect the mechanical constraints faced by humans and humanoid robots. In studies of humans, the ankle strategy seems to be used for small and slow perturbations on flat rigid support surfaces, while the hip strategy seems to be used for large or fast perturbations and on narrow or compliant support surfaces (Runge et al., 1999).

In this study in order to avoid the complexities associated with the dynamics of stepping as well as three-dimensional movements, the focus is limited to non-stepping, sagittal planar linkages with sagittal symmetry assumed, capable only for anterior/posterior movements of ankle, hip, and squat strategies, although the methodology may be used for medio-lateral movements as well, and may be extended to include stepping actions. External forces are gravitational forces applied to each segment at their center of mass (CoM), and the ground reaction force (GRF) applied to the feet segment at the center of pressure (CoP).

The control input to this system ($\boldsymbol{u}$) by which a person controls its posture is the set of torques applied on each joint: $\boldsymbol{u} = [T_{Ankle}\ T_{Knee} \dots]^T$, where T_{Ankle}, T_{Knee}, … are the torques applied from feet to shanks at the ankle, from shanks to thighs at the knee, etc. The number of the control input components (m) is equal to the number of model joints. The control input $\boldsymbol{u}$ is restricted by the individual's physical constraints such as the muscle strength, the necessity of keeping the feet stationary on the ground, etc. Let $\mathcal{U}$ be the feasible range of $\boldsymbol{u}$, which is an m-dimensional subset of $\mathbb{R}^m$ ($\mathcal{U} \subset \mathbb{R}^m$). $\mathcal{U}$ is specific to the subject. The control input constraint may be generally expressed in form of

$$\boldsymbol{u}(t) \in \mathcal{U};\ \forall t \quad \text{(2-1)}$$

Throughout this study we always deal with a conditions in the model dynamics so that the balance is maintained, and the dynamic equations is being solved always for such conditions. Since we have limited our scope into non-stepping mechanical model, one coherent condition for a successful control of balance is remaining the "feet" segment stationary on the ground. The equation of motion for such a general serial linkage with a fixed base of support may be expressed in the familiar form of

$$M(\boldsymbol{q})\ddot{\boldsymbol{q}} = C(\boldsymbol{q}, \dot{\boldsymbol{q}}) + G(\boldsymbol{q}) + \boldsymbol{u}$$

where $\boldsymbol{q}$ is the coordinate vector, which may be assumed as the joint angles:

$$\boldsymbol{q} = [\theta_{Ankle}\ \theta_{Knee} \dots]^T$$

and matrices M, C, and G are the inertial, Coriolis, and gravity terms. In order to describe the system ***state*** at a moment, a trivial way is to use the set of all joint angles and angular velocities, and show by $\boldsymbol{X}$:

$$\boldsymbol{X} = [\boldsymbol{q}^T\ \dot{\boldsymbol{q}}^T]^T$$

The state $\boldsymbol{x} = 0$ or the origin of the state space, hence, corresponds to the erect standing posture without any part of the body moving. The number of state variables (n) for the class of mechanical models considered in this study, therefore, is equal to the number of joints (m) times 2:

$$n = 2m$$

State space is then a virtual n-dimensional space, the axes of which are joint angles and angular velocities. Any body movement may be described by a curve (state trajectory) in the state space, showing what the body state is at every point in time. The state is also constrained to a region which is imposed by the range of motion of joints and so that it excludes a fall, which can be generally expressed by

$$\boldsymbol{X}(t) \in \mathcal{X};\ \forall t \quad \text{(2-2)}$$

where $\mathcal{X}$ is the feasible range of states which is an n-dimensional subspace of the state space including the origin ($\boldsymbol{x} = 0$). Let's assume that no joint has a range of motion including $+\pi$ or $-\pi$, which is, with a little approximation, a realistic assumption for humans in general movements. Particularly in standing balance studies, the practical range of motion of joints are much smaller that this assumption.

The equation of state for the general model of this work will be expressed in the general form of

$$\dot{\boldsymbol{X}}(t) = f\big(\boldsymbol{X}(t), \boldsymbol{u}(t)\big)\,; \boldsymbol{X}(0) = \boldsymbol{X_0} \quad \text{(2-3)}$$

In particular, in this research we use two mechanical models in order to describe the proposed methods, as well as to demonstrate how they can be used. The models are a 2-segment and a 3-segment model capable for ankle strategy and ankle and hip strategies of perturbation management and control of balance, respectively. The followings will introduce such models.

2.2. Two-segment model

Consider a well-known 2-segment mechanical model of the human standing balance consisting of the feet and the rest of body jointed at the ankle, with sagittal symmetry assumed, which supports forward-backward movements without taking steps. (Figure 2-1). Medial-lateral movements can be modeled with the same model with a similar story for balance in the frontal plane, and one may easily extend it to include both forward-backward and medial-lateral movements. This conventional model is widely in use as a platform in balance control analysis (see e.g. Geurtsen et al. 1975; Winter, 1995-b; Pai &

Patton, 1997; Hof et al. 2005; Pilkar et al. 2007; Honarvar and Nakashima, 2013). In particular, for nearly standing postures, where the distance of the CoM to the ground remains constant, the CoM does not move upward/downward, and the feet are kept horizontally in touch with the ground, human body dynamics may be completely described by the movement of its center of mass, and such a 2-segment model of human standing balance may be used to estimate the CoM dynamics.

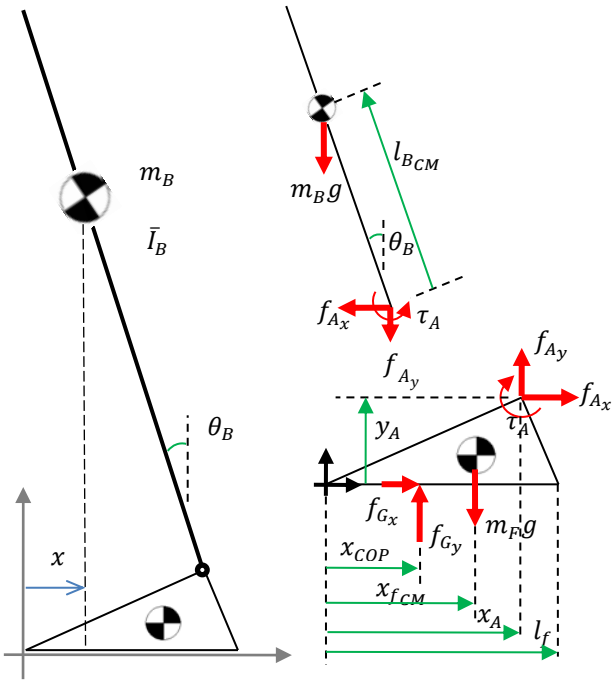

Figure 2-1. The 2-segment dynamical model we use in this research. It consists of two rigid parts: feet and the rest of body, jointed at ankle. External and internal forces, and the control input (ankle torque) are shown by red arrows.

Using such a sagittal model, an individual's situation at a moment (state) may be expressed uniquely by a set of 2 variables: location of the vertical projection of the CoM (x) and its time derivative (v), which uniquely correspond to the body inclination angle (θ_B) and its angular velocity ($\dot{\theta}_B$).

External forces on this system are: 1- the gravitational force which is applied to the body on its CoM, and 2- the ground reaction force which applies to the feet on the *center of pressure* (CoP). The CoP must remain always within the foot length, the vertical component of the ground reaction force must be always in an upward direction (pressure force), and its horizontal component must meet the static friction requirements.

The only control input to this model is the ankle torque, by which the individual may control their posture. The amount and direction of control input imposes the position of CoP. The control input for a certain individual is restricted by 2 extremes: the maximum strength in the dorsiflexion and the plantar flexion direction for that subject. These maximums vary with both the angle and angular velocity, because of 1- the muscle force-length and force-contraction rate dependency and 2- change of moment arm.

Ankle angle is limited to a given range of motion. We use some non-conservative data here in order to have the least restriction in our results due to the range of motion, which is based on Beers & Berkow (1999) and Anderson et al. (2007) and reckoned as -0.7*rad* (plantar flexed) to +0.50*rad* (dorsiflexed).

Writing the Newton equations for feet and body delivers the following four equations:

$$f_{G_x} = -m_B l_{B_{CM}} \left(\cos\theta_B \ddot{\theta_B} - \sin\theta_B \dot{\theta_B}^2\right) \qquad (2\text{-}4\text{-}1)$$

$$f_{G_y} = (m_F + m_B)g - m_B l_{B_{CM}} \left(\sin\theta_B \ddot{\theta_B} + \cos\theta_B \dot{\theta_B}^2\right) \quad (2\text{-}4\text{-}2)$$

$$m_B l_{B_{CM}}\left((x_A - x_{COP})\sin\theta_B - y_A\cos\theta_B\right)\ddot{\theta_B} + m_B l_{B_{CM}}\left((x_A - x_{COP})\cos\theta_B + y_A\sin\theta_B\right)\dot{\theta_B}^2 - \left(m_B x_A + m_F x_{f_{CM}} + (m_B + m_F)x_{COP}\right)g - \tau_A = 0 \quad (2\text{-}4\text{-}3)$$

$$\left(\overline{I}_B + m_B {l_{B_{CM}}}^2\right)\ddot{\theta_B} = m_B l_{B_{CM}}\sin\theta_B g + \tau_A \quad (2\text{-}4\text{-}4)$$

where f_{G_x}, f_{G_y}, and x_{COP} are the horizontal and vertical components of the ground reaction force and the location of the center of pressure, respectively, m_F, m_B, $\overline{I}_B$, $l_{B_{CM}}$, x_A, y_A, and $x_{f_{CM}}$ are feet mass, body mass, body standard moment of inertia, ankle to body CoM length, horizontal and vertical position of ankle with respect to toe, and horizontal position of the feet CoM, respectively, and τ_A is the torque applied from feet to the body at ankle. The acceleration of gravity is shown by g.

Equations (2-4-1) to (2-4-2) show the relationship between f_{G_x}, f_{G_y}, and x_{COP} with the body inclination angle (θ_B), its angular velocity ($\dot{\theta_B}$) and the applied torque (τ_A) at the moment. Equation (2-4-4) is the main dynamic equation which describes the dynamics of the system:

$$(2\text{-}4\text{-}4) \Rightarrow \ddot{\theta_B} = \frac{m_B l_{B_{CM}}}{\left(\overline{I}_B + m_B {l_{B_{CM}}}^2\right)} g\sin\theta_B + \frac{1}{\left(\overline{I}_B + m_B {l_{B_{CM}}}^2\right)}\tau_A \quad (2\text{-}5)$$

Now let's define the body state as the set of angle and angular velocity:

$$X_1 = \theta_B, X_2 = \dot{\theta_B} \Rightarrow \mathrm{X} = \begin{bmatrix}\theta_B \\ \dot{\theta_B}\end{bmatrix} \quad (2\text{-}6\text{-}1)$$

Therefore, the equation of state will be found easily as

$$\begin{cases}\dot{X_1} = X_2 \\ \dot{X_2} = a\sin X_1 + bu\end{cases} \quad (2\text{-}6\text{-}2)$$

where $u = \tau_A$, and

$$a = \frac{m_B l_{B_{CM}}}{\left(\overline{I}_B + m_B {l_{B_{CM}}}^2\right)} g > 0$$

$$b = \frac{1}{\left(\overline{I}_B + m_B {l_{B_{CM}}}^2\right)} > 0$$

The state of the system may be defined in another way as well. Define x as the location of the vertical projection of the body center of mass, and v as its time derivative, or the horizontal velocity of the center of mass

$$x = x_A - l_{B_{cm}} \sin\theta_B \quad (2\text{-}7\text{-}1)$$

$$v = -l_{B_{cm}} \dot{\theta}_B \cos\theta_B \quad (2\text{-}7\text{-}2)$$

and the normalized variables $\bar{x}$, $\bar{v}$, $\bar{u}$ as follows:

$$\bar{x} = \frac{x - x_A}{l_{B_{cm}}} \quad (2\text{-}8\text{-}1)$$

$$\bar{v} = \frac{v}{\sqrt{g l_{B_{cm}}}} \quad (2\text{-}8\text{-}2)$$

$$\bar{u} = \frac{u}{m_B g l_{B_{cm}}} \quad (2\text{-}8\text{-}3)$$

Now rewrite the dynamic equation (2-5) as

$$\ddot{\bar{x}} = \frac{\bar{v}^2 \bar{x}}{1 - \bar{x}^2} \frac{g}{l_{B_{cm}}} + c\bar{x}\sqrt{1 - \bar{x}^2} - \sqrt{1 - \bar{x}^2} du \quad (2\text{-}9)$$

where

$$c = \frac{1}{1 + \left(\frac{l_{B_g}}{l_{B_{cm}}}\right)^2} \frac{g}{l_{B_{cm}}}$$

$$d = \frac{1}{1 + \left(\frac{l_{B_g}}{l_{B_{cm}}}\right)^2} \frac{1}{m_B {l_{B_{cm}}}^2}$$

and define the body state Y as

$$Y_1 = \bar{x}, Y_2 = \bar{v} \Rightarrow \mathrm{Y} = \begin{bmatrix} \bar{x} \\ \bar{v} \end{bmatrix} \quad (2\text{-}10\text{-}1)$$

The equation of state for Y will be found as

$$\begin{cases} \dot{\bar{x}} = \bar{v}\sqrt{\dfrac{g}{l_{B_{cm}}}} \\ \dot{\bar{v}} = \sqrt{\dfrac{g}{l_{B_{cm}}}} \left(-\dfrac{\bar{x}}{1 - \bar{x}^2} \bar{v}^2 + \dfrac{1}{1 + \left(\dfrac{l_{B_g}}{l_{B_{cm}}}\right)^2} \sqrt{1 - \bar{x}^2} (\bar{x} - \bar{u}) \right) \end{cases}$$

or

$$\begin{cases} \dot{Y}_1 = \omega Y_2 \\ \dot{Y}_2 = \omega \left(-\frac{Y_1}{1-{Y_1}^2} {Y_2}^2 + \frac{1}{1+\left(\frac{l_{Bg}}{l_{B_{cm}}}\right)^2} \sqrt{1-{Y_1}^2}(Y_1 - \bar{u}) \right) \end{cases} \quad (2\text{-}10\text{-}2)$$

where

$$\omega = \sqrt{\frac{g}{l_{B_{cm}}}}$$

Because of the nature of the contact conditions between feet segment and the ground, as well as noting the condition of remaining the feet stationary on the ground, three constraints are imposed on the ground reaction force applied on feet:

1- The vertical component of the GRF must be upward, i.e. pressure type: $f_{G_y} \geq 0;\ \forall t$ (2-11-1)
2- The horizontal component of the GRF must comply with the static friction requirements:

$\left|f_{G_x}\right| \leq \mu_s f_{G_y}\ ;\ \forall t$ (2-11-2)

where μ_s is the static coefficient of friction.

3- Center of pressure must lie within the foot length (l_f):

$0 \leq x_{COP} \leq l_f\ ;\ \forall t$ (2-11-3)

These three conditions when incorporated with equations (2-4-1) to (2-4-3) come in this form:

$$\frac{(m_F+m_B)}{m_B l_{B_{CM}}} g \geq \left(\sin\theta_B \ddot{\theta}_B + \cos\theta_B \dot{\theta_B}^2\right) \quad (2\text{-}12\text{-}1)$$

$$\left|\cos\theta_B \ddot{\theta}_B - \sin\theta_B \dot{\theta_B}^2\right| \leq \mu_s \left(\frac{(m_F+m_B)}{m_B l_{B_{CM}}} g - \left(\sin\theta_B \ddot{\theta}_B + \cos\theta_B \dot{\theta_B}^2\right)\right) \quad (2\text{-}12\text{-}2)$$

$$0 \leq \tau_A + \left(-m_B l_{B_{CM}} \left(\sin\theta_B \ddot{\theta}_B + \cos\theta_B \dot{\theta_B}^2\right) x_A + m_B l_{B_{CM}} \left(\cos\theta_B \ddot{\theta}_B - \sin\theta_B \dot{\theta_B}^2\right) y_A + \left(m_F x_{f_{CM}} + m_B x_A\right) g\right) \leq f_{G_y} l_f \quad (2\text{-}12\text{-}3)$$

Equation (2-4-4) relates τ_A and θ_B to $\ddot{\theta}_B$. Thus, at every state (X or Y) three constraints of (2-12) restrict the applicable ankle torque, and they must be satisfied together. These are referred to as the "foot constraints" throughout this work.

2.3. Three-segment model

Consider a 3-segment model consisting of feet, lower limbs excluding feet which is called "Legs", and the upper body (head, arms, and trunk) which is called "HAT", jointed at the ankle and hip (Figure 2-2). Symmetry in sagittal plane is assumed. External forces are:

1) gravitational force applied to the feet, Legs, and HAT at their CoMs, and 2) a ground reaction force (GRF) applied to the feet at the CoP. The control inputs into this model are ankle and hip torques, by which the individual controls his or her posture.

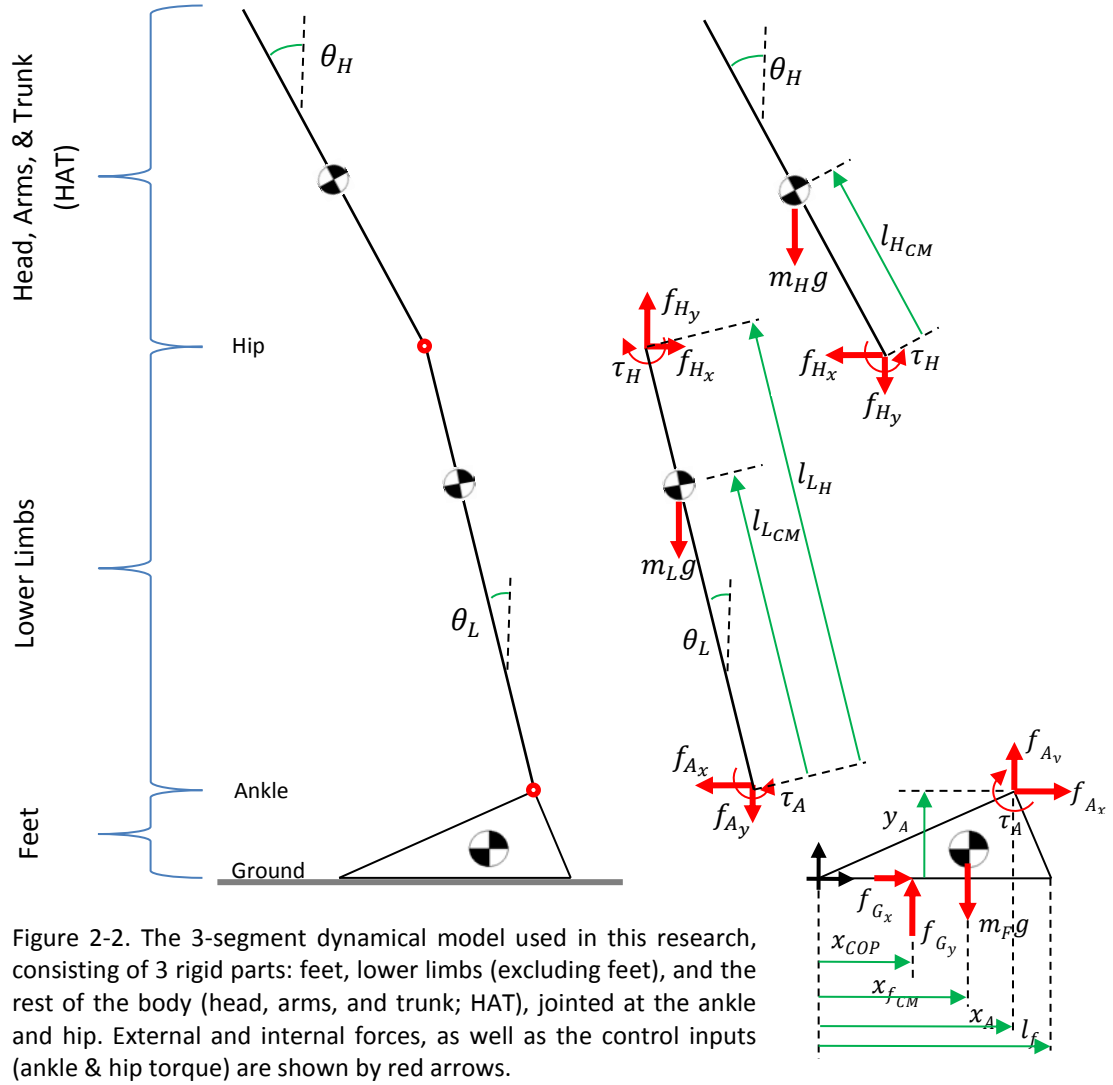

Figure 2-2. The 3-segment dynamical model used in this research, consisting of 3 rigid parts: feet, lower limbs (excluding feet), and the rest of the body (head, arms, and trunk; HAT), jointed at the ankle and hip. External and internal forces, as well as the control inputs (ankle & hip torque) are shown by red arrows.

Writing the Newton equations for feet and body delivers the following four equations:

Foot:
$$\begin{cases} f_{G_x} + f_{A_x} = 0 \\ f_{G_y} + f_{A_y} - m_F g = 0 \\ f_{A_y}(x_A - x_{COP}) - m_F g(x_{f_{CM}} - x_{COP}) - f_{A_x} y_A - \tau_A = 0 \end{cases}$$

Legs:
$$\begin{cases} -f_{A_x} + f_{H_x} = -m_L l_{L_{CM}} \left(\cos\theta_L \ddot{\theta}_L - \sin\theta_L \dot{\theta_L}^2\right) \\ -f_{A_y} + f_{H_y} - m_L g = -m_L l_{L_{CM}} \left(\sin\theta_L \ddot{\theta}_L + \cos\theta_L \dot{\theta_L}^2\right) \\ \bar{I}_L \ddot{\theta}_L = -f_{A_x} l_{L_{CM}} \cos\theta_L - f_{A_y} l_{L_{CM}} \sin\theta_L - f_{H_x}(l_{L_H} - l_{L_{CM}})\cos\theta_L - f_{H_y}(l_{L_H} - l_{L_{CM}})\sin\theta_L + \tau_A - \tau_H \end{cases}$$

$$\text{HAT: } \begin{cases} f_{H_x} = m_H\left(l_{L_H}\left(\cos\theta_L\ddot{\theta_L} - \sin\theta_L\dot{\theta_L}^2\right) + l_{H_{CM}}\left(\cos\theta_H\ddot{\theta_H} - \sin\theta_H\dot{\theta_H}^2\right)\right) \\ f_{H_y} + m_H g = m_H\left(l_{L_H}\left(\sin\theta_L\ddot{\theta_L} + \cos\theta_L\dot{\theta_L}^2\right) + l_{H_{CM}}\left(\sin\theta_H\ddot{\theta_H} + \cos\theta_H\dot{\theta_H}^2\right)\right) \\ \bar{I}_H\ddot{\theta}_H = -f_{H_x}l_{H_{CM}}\cos\theta_H - f_{H_y}l_{H_{CM}}\sin\theta_H + \tau_H \end{cases}$$

where $f_{G_x}, f_{G_y}, f_{A_x}, f_{A_y}, f_{H_x}, f_{H_y}$ are the horizontal and vertical components of the GRF, horizontal and vertical components of the force the foot part exerts on the Legs part at ankle joint, and horizontal and vertical components of the force the Legs part exerts on the HAT part at hip joint, respectively. Angles θ_L and θ_H are the inclination angle of Legs and HAT with respect to the vertical line, respectively. By eliminating $f_{A_x}, f_{A_y}, f_{H_x}, f_{H_y}$ from the above equations we will have the below three equations:

$$\begin{aligned} f_{G_x} = -f_{A_x} = &-\left(m_H l_{L_H} + m_L l_{L_{CM}}\right)\cos\theta_L\ddot{\theta_L} - \left(m_H l_{H_{CM}}\right)\cos\theta_H\ddot{\theta_H} \\ &+ \left(m_H l_{L_H} + m_L l_{L_{CM}}\right)\sin\theta_L\dot{\theta_L}^2 + \left(m_H l_{H_{CM}}\right)\sin\theta_H\dot{\theta_H}^2 \end{aligned}$$

$$\begin{aligned} f_{G_y} = -f_{A_y} + m_F g \\ = &-\left(m_H l_{L_H} + m_L l_{L_{CM}}\right)\sin\theta_L\ddot{\theta_L} - \left(m_H l_{H_{CM}}\right)\sin\theta_H\ddot{\theta_H} \\ &- \left(m_H l_{L_H} + m_L l_{L_{CM}}\right)\cos\theta_L\dot{\theta_L}^2 - \left(m_H l_{H_{CM}}\right)\cos\theta_H\dot{\theta_H}^2 \\ &+ \left(m_F + m_L + m_H\right)g \end{aligned}$$

$$\begin{aligned} \tau_A = -y_A\Big[&m_L l_{L_{CM}}\left(\cos\theta_L\ddot{\theta_L} - \sin\theta_L\dot{\theta_L}^2\right) \\ &+ m_H\left(l_{L_H}\left(\cos\theta_L\ddot{\theta_L} - \sin\theta_L\dot{\theta_L}^2\right) + l_{H_{CM}}\left(\cos\theta_H\ddot{\theta_H} - \sin\theta_H\dot{\theta_H}^2\right)\right)\Big] \\ &+ \left(x_A - x_{COP}\right)\Big[m_L\left(-g + l_{L_{CM}}\left(\sin\theta_L\ddot{\theta_L} + \cos\theta_L\dot{\theta_L}^2\right)\right) \\ &+ m_H\left(-g + l_{L_H}\left(\sin\theta_L\ddot{\theta_L} + \cos\theta_L\dot{\theta_L}^2\right) + l_{H_{CM}}\left(\sin\theta_H\ddot{\theta_H} + \cos\theta_H\dot{\theta_H}^2\right)\right)\Big] \\ &- m_F g\left(x_A - x_{f_{CM}}\right) \end{aligned}$$

(2-13)

in addition to the two equations which form the main dynamic equation of the system expressed as

$$M(q)\ddot{q} = C(q,\dot{q}) + G(q) + u$$

where q is the coordinate vector

$$q = [\theta_L\ \theta_H]^T$$

and u is the control input vector. Matrices M, C, and G are the inertial, Coriolis, and gravity terms as follows:

$$M(q) = \begin{bmatrix} \bar{I}_L + m_L l_{L_{CM}}^2 + m_H l_{L_H}^2 & m_H l_{L_H} l_{H_{CM}}\cos(\theta_H - \theta_L) \\ m_H l_{L_H} l_{H_{CM}}\cos(\theta_H - \theta_L) & \bar{I}_H + m_H l_{H_{CM}}^2 \end{bmatrix}$$

$$C(q,\dot{q}) = \begin{bmatrix} 0 & \left(m_H l_{L_H} l_{H_{CM}} \sin(\theta_H - \theta_L)\right) \\ -\left(m_H l_{L_H} l_{H_{CM}} \sin(\theta_H - \theta_L)\right) & 0 \end{bmatrix} \begin{bmatrix} \dot{\theta_L}^2 \\ \dot{\theta_H}^2 \end{bmatrix}$$

$$G(q) = \begin{bmatrix} \left(m_L l_{L_{CM}} + m_H l_{L_H}\right)\sin\theta_L \\ m_H l_{H_{CM}} \sin\theta_H \end{bmatrix} g$$

$$u = \begin{bmatrix} \tau_A - \tau_H \\ \tau_H \end{bmatrix}$$

(2-14)

The three foot constraints due to the contact conditions between feet and the ground exist in this model similar to the foot constraints (2-11) in the two-segment model, as follows:

$$f_{G_y} \geq 0;\ \forall t$$

$$\left|f_{G_x}\right| \leq \mu_s f_{G_y}\ ;\ \forall t$$

$$0 \leq x_{COP} \leq l_f\ ;\ \forall t$$

which when incorporated with equations (2-13) and (2-14) set restrictions on the applicable ankle and hip torques at every body state. Such constraints are to be satisfied in addition to the limitations due to the body mechanical strength (mainly the muscles strength).

The body state (X) at a moment may be uniquely expressed by a 4-variable set: Legs and HAT inclination angles and their angular velocities; $X = [q^T \quad \dot{q}^T]^T = [\theta_L \quad \theta_H \quad \dot{\theta}_L \quad \dot{\theta}_H]^T$. The equation of state may be written in the general form of

$$\dot{X}(t) = f\big(X(t), u(t)\big)\ ;\ X(0) = X_0$$

where

$$f_{1:2,1:4}\big(X(t), u(t)\big) = [0 \quad I]X(t)$$

$$f_{3:4,1:4}\big(X(t), u(t)\big) = M^{-1}(q)\big(C(q,\dot{q}) + G(q)\big) + M^{-1}(q)u(t)$$

2.4. Summary

In this section we specified the class of mechanical models being used in this research, which is limited to the non-stepping models and those described only in the sagittal plane. In particular, a 2-segment and a 3-segment body model are introduced which are capable for ankle strategy and ankle and hip strategies of perturbation management and control of balance, respectively. These models are used in this research in order to describe the proposed methods, as well as to demonstrate how they can be used.

Chapter 3
The Balanceable Region

3.1. Introduction

This section addresses the question of what condition is to be fulfilled for the balance to be maintained during a movement or task, or similarly, what is the range of body movements in which the control of balance will be feasible.

We propose a new method to figure out the feasible range of the movement states in which control of balance would be possible, for an arbitrarily given mechanical characteristics of an individual. In the followings, the "balanceable region" will defined first, then the idea behind our suggested method will be illustrated by step-by-step solving the balanceable region for a simple mechanical model. In the following the balance recovery problem and the concept of balanceable region will be defined first, then the key idea will be described on a very simple mechanical model. Next, the theory and theorems for a more generic model will be formulated, followed by application of the method on a 2-segment and a 3-segment mechanical model, and a discussion on the method, results, and limitations.

3.2. The balanceable region

Human body is being regarded as a mechanical linkage including joint actuators. Control input in this model is the set of joint torques. An unconstrained control input being assumed, any initial state can be controlled and driven to the erect standing posture without any part of the body moving (origin of the state space). However in the reality the applicable joint torques are restricted by the individual's physical constraints mainly including the muscles strength, and the necessity of keeping the feet stationary on the ground.

The balance recovery problem, the problem of driving the system state from an initial state ($\boldsymbol{x_0}$) at time $t = 0$ to the balance posture ($\boldsymbol{x} = 0$, the origin of the state space) in some limited time (t_f), is finding a control input over the time (control input trajectory) to be applied into the equation of state (2-3) which drives the body state to the origin while satisfying the control input constraint (2-1), as well as the state constraint (2-2), during the entire recovery movement. Because of the constraints, the balance recovery problem has a solution for some initial states and is not solvable at some other initial states.

Maintaining the balance from an initial state $\boldsymbol{x_0}$ for a certain individual who has its own specific input constraint $\mathcal{U}$ is feasible, or it can be called $\boldsymbol{x_0}$ *is balanceable for* $\mathcal{U}$, if and only if the corresponding balance recovery problem has a solution. In other words, an initial state for a human body model with given properties is balanceable, if and only if the system is able to drive that state to the balance posture satisfying all the necessary constraints during the recovery movement from beginning to the end:

$\boldsymbol{x_0}$ is balanceable $\Longleftrightarrow \exists u(t) \in \mathcal{U};\ \forall t \geq 0$ such that

$$\begin{cases} x(t) \in \mathcal{X};\ \forall t \geq 0 \\ x(t_{\mathrm{f}}) = 0;\ t_{\mathrm{f}} \geq 0 \end{cases} \text{ subject to } \dot{x} = f(x,u); x(0) = x_0$$

where $\mathcal{U} \subset \mathbb{R}^m$is the input constraint (m is the input vector size) and $\mathcal{X} \subset \mathbb{R}^n$ is the state constraint (n is the state dimension), and $\dot{x} = f(x,u)$ shows the equation of state for the mechanical model.

Let $\mathcal{B}(\mathcal{U})$ be the set of all states (subspace of the state space) that are balanceable for $\mathcal{U}$, and call it the *balanceable region* of $\mathcal{U}$. It means that for a mechanical model with certain anatomical parameters, if the control input is constrained to take values only from the set $\mathcal{U}$, the balanceable region $\mathcal{B}(\mathcal{U})$ shows from which body configurations (including the velocity of segments) the control of balance would be possible. At any other state, i.e. $\mathbb{R}^n - \mathcal{B}$, a fall will initiate. Obviously, the balanceability of a state depends on the mechanical properties of the individual (more precisely, the physical properties of the mechanical model of the body), such as the geometric and inertial parameters, as well as the control input and state constraints. For example, a more strong individual has a larger feasible input region $\mathcal{U}$, and thus has a larger balanceable region $\mathcal{B}$.

3.3. Finding the balanceable region on a simple model

A trivial method to obtain the balanceable region $\mathcal{B}$ for a model with given anatomical parameters and given input constraint $\mathcal{U}$ is to solve the balance recovery problem for many states scattered (intelligently) in the state space, in order to find which states are balanceable. Checking the balanceability for a single state is a time consuming process, since an iterative searching algorithm should try different control input trajectories (not control input points), apply each to the dynamic model and follow the resultant state trajectory. When such an algorithm is to be repeated for so many initial states, the computational burden becomes very huge. Such an algorithm is computationally very expensive, in particular when the dimension of the state space increases.

However, fortunately there is a possibility to dramatically reduce the computational load of such a huge numerical method. Let's illustrate the idea on a very simple mechanical model. Suppose a simple inverted pendulum (Figure 3-1) with an equation of motion of

$$\ddot{\theta} = a\sin\theta + b\tau \ ;\ a = \frac{mgr_{cm}}{(I_{cm} + mr_{cm}{}^2)} \ , \qquad b = \frac{1}{(I_{cm} + mr_{cm}{}^2)}$$

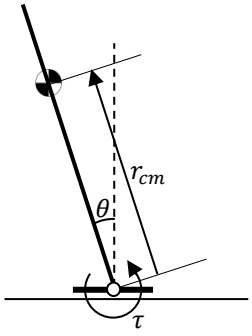

Figure 3-1.The mechanical model used to illustrate the idea behind the analytic finding of the balanceable region. It is a simple inverted pendulum.

To simulate an average human of $m = 75\ [kg]$ and $H = 1.75\ [m]$, one may estimate the model parameters based on the anthropometric data in Winter (2009) as bellow:

$r_{cm} = (1 - 0.412)H = 1.0290$; Position of CG, from heel

$I_{total} = I_{legs} + I_{HAT} = 9.8687 + 49.4622 = 59.3309$; Moment of inertia of whole body with respect to the heel joint.

$$\Rightarrow \begin{cases} a = 12.760 \\ b = 0.0169 \end{cases}$$

Control input (u) is the applied torque, and let the state (x) for this system be the angle and angular velocity:

$$\begin{cases} x_1 \coloneqq \theta \\ x_2 \coloneqq \dot{\theta} \\ u \coloneqq \tau \end{cases}$$

The equation of state will be

$$\begin{cases} \dot{x_1}(t) = x_2(t) \\ \dot{x_2}(t) = a\sin x_1(t) + bu(t) \end{cases} ; \begin{cases} x_1(0) = x_{1_0} \\ x_2(0) = x_{2_0} \\ t \in \mathbb{R}^+ + \{0\} \end{cases}$$ (Eq. of State in continuous form) (3-1)

where $\left[x_{1_0}, x_{2_0}\right]^T$ is the initial state.

Due to physical restrictions the applicable torque is limited to some range (control input constraint). Let's roughly estimate the input constraint (based on the anthropometric data in Winter, 2009) as follows:

$$L_{fF} + L_{fR} = 0.152H = 0.266$$

$$L_{fF} = 0.266 \times \frac{2.5}{3.5} = 0.190$$

$$L_{fR} = 0.266 \times \frac{1}{3.5} = 0.076$$

$$N_{max} = m(1.1g) = 809.3$$

where L_{fF}, L_{fR}, and N_{max} are the horizontal distance between ankle and toe, horizontal distance between ankle and heel, and the maximum normal ground reaction force in quite standing and small movements around it. The maximum torque applied to the body in plantar flexion direction ($u_{PF_{max}}$) cannot exceed the torque produced by the GRF when the center of pressure is located at its most forward location (toe), therefore:

$$u_{PF_{max}} = L_{fF}N_{max} = 153.7718$$

and similarly, the maximum torque in dorsiflexion direction ($u_{DF_{max}}$) will be the product of N_{max} and L_{fR}:

$$u_{DF_{max}} = L_{fR}N_{max} = 61.5087$$

By selecting the dorsiflexion as the positive direction for torques, the control input constraint for such a model may be defined as

$$-153.7718 \leq u \leq +61.5087 \quad (3\text{-}2)$$

Now suppose system (3-1) without applying any control input (zero-input system)

$$\begin{cases} \dot{x_1}(t) = x_2(t) \\ \dot{x_2}(t) = a\sin x_1(t) \end{cases} \quad (3\text{-}3)$$

and draw the phase plane (state trajectories from different initial states, in $x_1 - x_2$ space) for this system.

The equilibrium point for system (3) is $x_{eq} = \begin{bmatrix} 0 \\ 0 \end{bmatrix}$. Write the Taylor's expansion with respect to the equilibrium point:

$$\dot{x} = \begin{bmatrix} x_2(t) \\ a\sin x_1(t) \end{bmatrix} = f(x) = f(x_{eq}) + \left.\frac{\partial f(x)}{\partial x}\right|_{x=x_{eq}} (x - x_{eq}) + O((x - x_{eq})^2)$$

$f(x_{eq}) = 0$, and for points around the equilibrium point one may linearize the dynamics and estimate it as

$$\dot{x} = Ax = \begin{bmatrix} 0 & 1 \\ a & 0 \end{bmatrix} x \quad (3\text{-}4)$$

Find the eigenvalues and eigenvectors for system (3-4):

$$|\lambda I - A| = 0 \Longrightarrow \begin{cases} \lambda_1 = -\sqrt{a} \\ \lambda_2 = +\sqrt{a} \end{cases} \rightarrow \begin{cases} v_1 = \begin{bmatrix} 1 \\ -\sqrt{a} \end{bmatrix} \rightarrow stable \\ v_2 = \begin{bmatrix} 1 \\ +\sqrt{a} \end{bmatrix} \rightarrow unstable \end{cases}$$

So, since a is an absolutely positive scalar, system (3-4) has one positive (stable) and one negative (unstable) eigenvalue. So the origin of the phase plane is unstable of saddle type for system (3-4) as well as the nonlinear system (3-3), and there is one stable manifold along with the stable eigenvector, and one unstable manifold along with the unstable eigenvector. Phase plane for system (3-3) is shown in Figure 3-2.

It is trivial that the stable manifold of system (3-3) is totally included in the balanceable region of system (3-1) with the control input constraint of (3-2). In addition, if some control input which satisfies the constraint can drives the system from an initial point to any point on the stable manifold, that initial state is balanceable (see Figure 3-3). In other words, if a

trajectory produced by some allowed control input cuts through the stable manifold, that trajectory entirely lies inside the balanceable region.

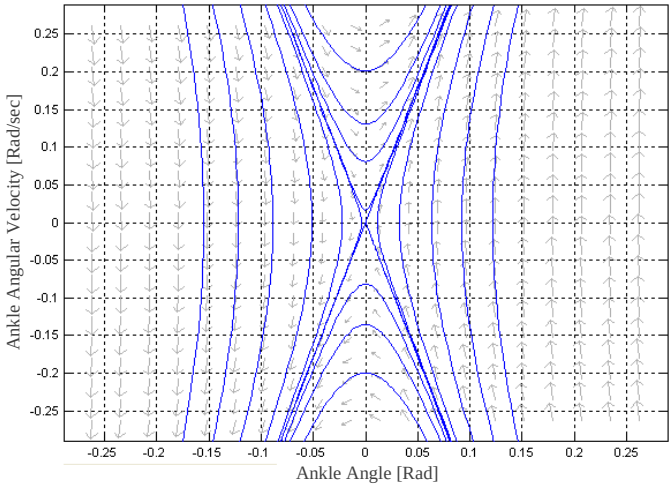

Figure 3-2. phase-plane for the zero-input nonlinear system (3-3).

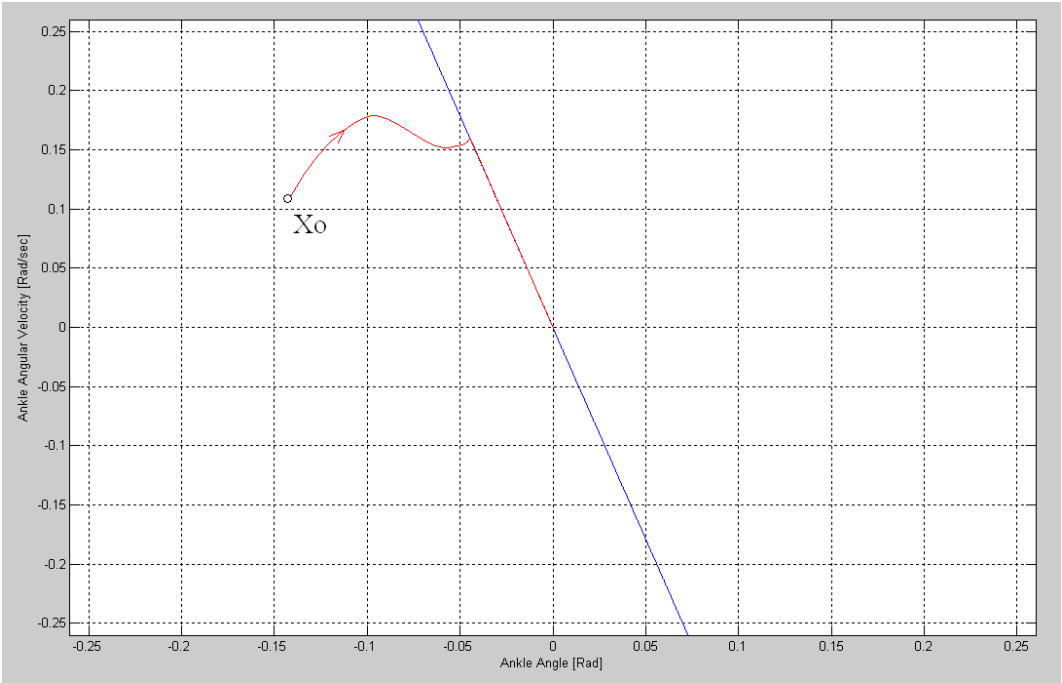

Figure 3-3. Blue curve: stable manifold for the zero-input system (3-3). If a trajectory (red curve) meets this manifold, by setting input to zero it will go to the origin.

Now suppose system (3-1) with the maximum plantar flexion torque ($u_{PF_{max}}$) applied on it:

$$\begin{cases} \dot{x_1}(t) = x_2(t) \\ \dot{x_2}(t) = a\sin x_1(t) + bu_{PF_{max}} \end{cases} \quad (3\text{-}5)$$

Let's draw the phase plane for this system. First, find the equation of state trajectories:

$\frac{dx_2}{dx_1} = \frac{a\sin x_1(t) + bu_{PF_{max}}}{x_2(t)}$; for $x_2(t) \neq 0$

$$x_2(t)dx_2 = \left(a\sin x_1(t) + bu_{PF_{max}}\right) dx_1$$

$$x_2{}^2(t) = -2a\left(\cos(x_1(t)) - \cos\left(x_{1_0}\right)\right) + 2bu_1\left(x_1(t) - x_{1_0}\right) + x_{2_0}{}^2 \; ; \; x_2(t) \neq 0 \quad (3\text{-}6)$$

where $x_0 = [x_{1_0} \quad x_{2_0}]^T$ is the initial state, or a given state a trajectory has to pass through. The phase plane for system (3-5) is shown in Figure 3- 4. The equilibrium point for this system is:

$$\dot{x} = \begin{bmatrix} x_2(t) \\ a\sin x_1(t) + bu_{PF_{max}} \end{bmatrix} = 0 \Longrightarrow x_{eq} = \begin{bmatrix} \sin^{-1}\left(-\frac{b}{a}u_{PF_{max}}\right) \\ 0 \end{bmatrix} ; \text{ for } -\frac{a}{b} \leq u_{PF_{max}} \leq \frac{a}{b}$$

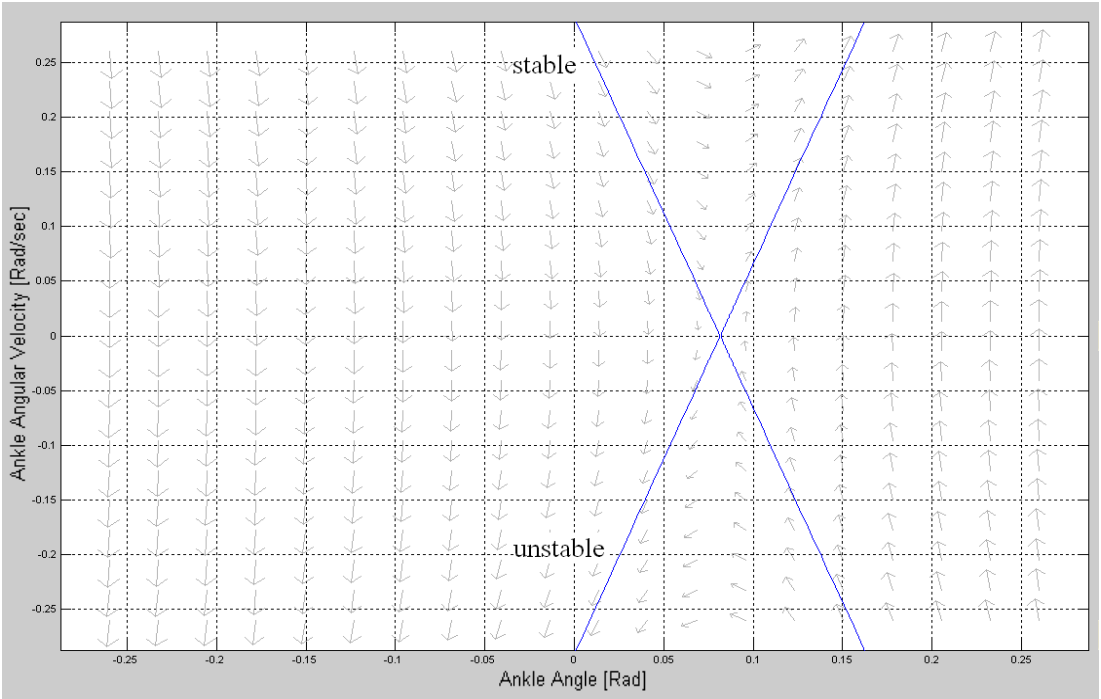

Figure 3-4. Phase-plane and stable and unstable manifolds for system (3-5)

Equation of state trajectories (3-6) passing through this equilibrium point (in limit, not exactly passing through the equilibrium point) has two solutions. By a variable change from x to y where

$$y \coloneqq x - x_{eq} = \begin{bmatrix} x_1 - \sin^{-1}\left(-\frac{b}{a}u_{PF_{max}}\right) \\ x_2 \end{bmatrix}$$

system (5) comes in form of

$$\dot{y} = \dot{x} = \begin{bmatrix} x_2 \\ a\sin x_1 + bu_{PF_{max}} \end{bmatrix} = \begin{bmatrix} y_2 \\ asin\left(y_1 + \sin^{-1}\left(-\frac{b}{a}u_{PF_{max}}\right)\right) + bu_{PF_{max}} \end{bmatrix}$$

with an equilibrium point at the origin:

$$y_{eq} = \begin{bmatrix} 0 \\ 0 \end{bmatrix}$$

and the linearized system around this equilibrium point comes in form of

$$\dot{y} = Ay$$

where

$$A = \frac{\partial f(y, u_1)}{\partial y}\bigg|_{y=y_{eq}} = \begin{bmatrix} 0 & 1 \\ \sqrt{a^2 - b^2 {u_{PF_{max}}}^2} & 0 \end{bmatrix}$$

This system, hence, has one stable and one unstable eigenvalue:

$$\begin{cases} \lambda_1 = -\sqrt[4]{a^2 - b^2 {u_{PF_{max}}}^2} \rightarrow stable \\ \lambda_2 = +\sqrt[4]{a^2 - b^2 {u_{PF_{max}}}^2} \rightarrow unstable \end{cases}$$

and accordingly one stable and one unstable eigenvector:

$$\begin{cases} v_1 = \begin{bmatrix} 1 \\ -\sqrt[4]{a^2 - b^2 {u_{PF_{max}}}^2} \end{bmatrix} \rightarrow stable \\ v_2 = \begin{bmatrix} 1 \\ +\sqrt[4]{a^2 - b^2 {u_{PF_{max}}}^2} \end{bmatrix} \rightarrow unstable \end{cases}$$

Thus, the stable subspace of system (3-5) is the solution of equation (3-6) for its equilibrium point, which aligns with the stable eigenvector of the linearized system around its equilibrium point. Figure 3-4 shows both stable and unstable subspaces (manifolds) of system (3-5). As it is clear in this figure, all states between the stable manifold of system (3-5) and stable manifold of system (3-3) cut through the stable manifold of system (3-3) under dynamics of (3-5). So, since dynamics (3-5) satisfies the constraint (3-2), this area is entirely included in the balanceable region of system (3-1) with constraint (3-2).

A similar story concludes that the area between the stable manifold of system

$$\begin{cases} \dot{x_1}(t) = x_2(t) \\ \dot{x_2}(t) = a\sin x_1(t) + bu_{DF_{max}} \end{cases} \quad (3\text{-}7)$$

and the stable manifold of system (3-3) is entirely balanceable, which concludes to that the area between stable manifolds of systems (3-5) and (3-7) are included in the balanceable region of system (3-1) with constraint (3-2). Phase plane for system (3-7) as well as its stable and unstable manifolds is shown in Figure 3-5. Figure 3-6 shows the stable subspaces for systems (3-3), (3-5), and (3-7). The highlighted area is totally balanceable.

At a point outside this area, the system with an input of either of $u_{PF_{max}}$ and $u_{DF_{max}}$ have the state trajectories outward of this region (note to the arrows in Figure 3-4 and 3-5).

It can be easily shown that the situation is the same for any other control input within the range of $[-153.7718 \sim +61.5087]$, which means there is no possibility to drive a state outside of the area between the stable manifolds for systems (3-5) and (3-7), inside this area, with a torque satisfying the constraint (3-2). The conclusion is, the balanceable region for system (3-1) with input constraint of (3-2) is equal to the region between stable manifolds of system (3-5) and (3-7).

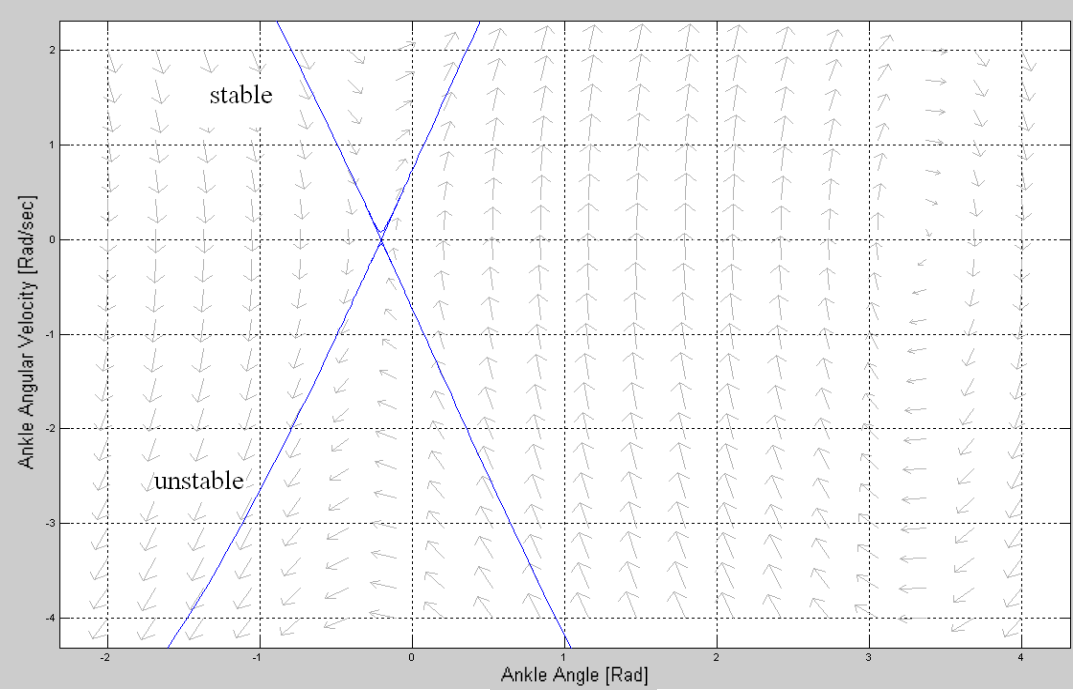

Figure 3-5. Phase-plane and stable and unstable manifolds for system (3-7)

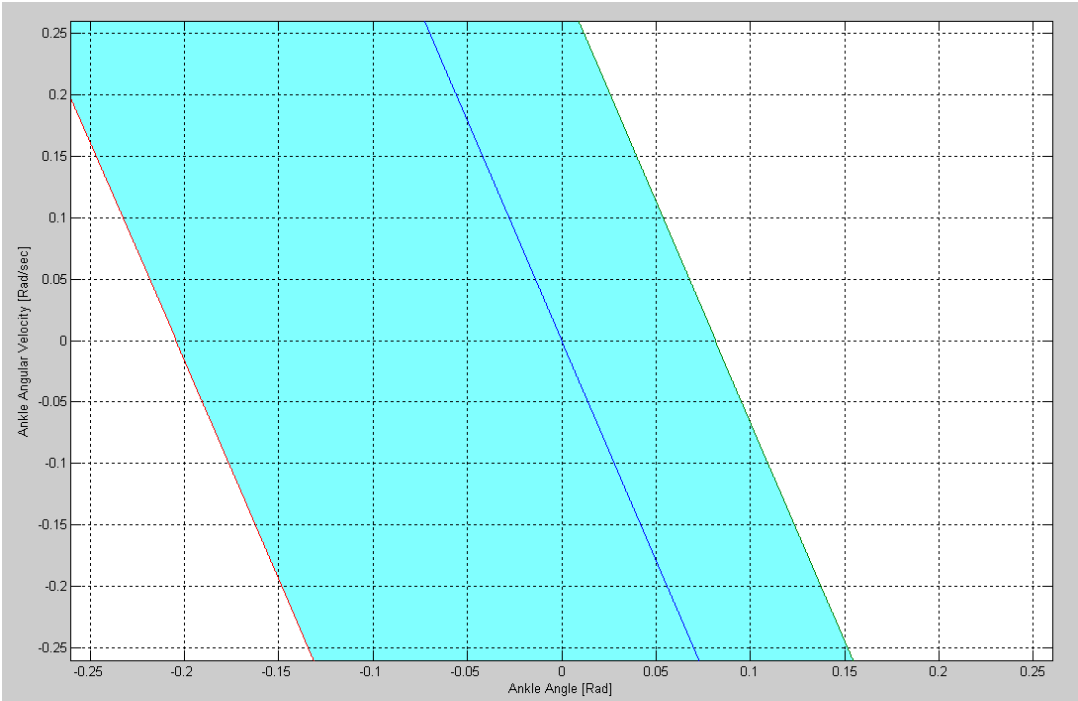

Figure 3-6. Green and red curves are the stable manifolds for system (3-5) and system (3-7), respectively.. Balanceable region for system (3-1) is the area between the green and red curves. Blue curve is the stable manifold for system (3-3)

The balanceable region for a simple mechanical model of human body is obtained analytically, without using a huge numerical method of checking the balanceability for many initial states and drawing the balanceable region from the results. In the followings, the idea will be formulated so that can be used for more general mechanical models.

3.4. The balanceable region for a generic non-stepping model

In the following, for a general non-stepping mechanical model in the sagittal plane, a specific region will be introduced as a subspace of the state space which may be analytically defined and found for any control input constraint, and it will be shown that it is the balanceable region.

The integrated stable subspace (*ISS*): System (2-3) with $\boldsymbol{u}(t) = 0$ has an equilibrium point at zero ($\boldsymbol{x_{eq}} = 0$), i.e. the system is in equilibrium if all of the joint angles and angular velocities are zero. This equilibrium point is unique in $\mathcal{X}$ if $\mathcal{X}$ includes no point with an angle equal to $\pm\pi$. Such an assumption has already been made on the feasible state region $\mathcal{X}$. Also, $\boldsymbol{x_{eq}} = 0$ is an unstable equilibrium point (since a small perturbation will not automatically return to the equilibrium unless a controller makes it stable) with an n_S-dimensional stable subspace (SS) and n_U-dimensional unstable subspaces, where $n_S + n_U = n$. Similarly, System (2-3) for any constant input $\boldsymbol{u}(t) \equiv \boldsymbol{u_1}$ has an equilibrium point $\boldsymbol{x_{eq}}(\boldsymbol{u_1})$ in $\mathcal{X}$. Let $SS(\boldsymbol{u_1})$ represent the corresponding stable subspace.

Let's assume that for every input $\boldsymbol{u}^*$ on the boundary of the input constraint $\mathcal{U}^*$ there exists an equilibrium point $\boldsymbol{x_{eq}}$ such that $f(\boldsymbol{x_{eq}}, \boldsymbol{u}^*) = 0$ (This assumption will be discussed later). Define the Integrated Stable Subspaces (*ISS*) as:

$$ISS(\mathcal{U}) = \cup\{SS(\boldsymbol{u}^*) | \boldsymbol{u}^* \in \mathcal{U}^*\}$$

which is a piecewise continuous $n-1$ dimensional subspace of the state space. *ISS* divides $\mathcal{X}$ into three regions: on *ISS*, inside (including the origin) which we show by *iISS*, and outside (*oISS*).

Theorem 1: Under the system dynamics of (2-3) with its input and state constrained to $\mathcal{U}$ and $\mathcal{X}$, respectively, any state in $iISS(\mathcal{U})$ will be able to be controlled so as not to escape out of $iISS(\mathcal{U})$:

$$\forall \boldsymbol{x_0} \in iISS(\mathcal{U})\ \exists \boldsymbol{u}(t) \in \mathcal{U} \text{ such that } \forall t > 0: \boldsymbol{x}(t) \in ISS(\mathcal{U}) \cup iISS(\mathcal{U})$$

Proof: For any point $\boldsymbol{p}$ on $ISS(\mathcal{U})$ there exists an input $\boldsymbol{u_p}$ on the boundary of $\mathcal{U}$ (which is shown by $\mathcal{U}^*$) the corresponding equilibrium point of which ($\boldsymbol{x_{eq}}(\boldsymbol{u_p})$) is on $ISS(\mathcal{U})$ and $\boldsymbol{p}$ is on its stable subspace ($SS(\boldsymbol{u_p})$):

$$\boldsymbol{p} \in ISS(\mathcal{U}) \Longrightarrow \exists \boldsymbol{u_p} \in \mathcal{U}^*, \boldsymbol{x_{eq}}(\boldsymbol{u_p}) \in ISS(\mathcal{U}) : \boldsymbol{p} \in SS(\boldsymbol{u_p})$$

This is equivalent to the idea that every point on ISS lies on the SS of some $\boldsymbol{u_p} \in \mathcal{U}^*$ which entirely lies on $ISS(\mathcal{U})$, and this is the definition of ISS. Therefore, $\boldsymbol{p}$ will remain on

$SS(\boldsymbol{u_p})$ and will be driven to $\boldsymbol{x_{eq}}(\boldsymbol{u_p})$ simply by setting the control input as $\boldsymbol{u}(t) \equiv \boldsymbol{u_p} \in \mathcal{U}^*$. The result is, hence, as a trajectory touches ISS, it can be controlled to remain on it. Thus, an individual with an input constraint of $\mathcal{U}$ can control its state to remain on or in $ISS(\mathcal{U})$ if it is on or in $ISS(\mathcal{U})$. ***

However, $iISS$ is not necessarily a bounded set, so if the state is remaining in $iISS$ it doesn't necessarily mean that it goes toward the origin, or even that it doesn't get infinitely far. Another step forward is needed:

Theorem 2: Suppose there is a control input constraint $\mathcal{U}_1$ and a control input constraint $\mathcal{U}_2$ entirely inside $\mathcal{U}_1$, i.e. $\mathcal{U}_2 \subset (\mathcal{U}_1 - {\mathcal{U}_1}^*)$ where ${\mathcal{U}_1}^*$ is the boundary of $\mathcal{U}_1$. It may be easily proven that the integrated stable subspaces of $\mathcal{U}_2$ entirely lies inside that of $\mathcal{U}_1$, i.e. $ISS(\mathcal{U}_2) \subset iISS(\mathcal{U}_1)$. Then, if $\mathcal{U}_1$ is not the zero-set ($\mathcal{U}_1 \neq \{0\}$), for every point $\boldsymbol{p_2}$ on $ISS(\mathcal{U}_2)$ there exist a control input $\boldsymbol{u_1}$ on $\mathcal{U}_1$, another control input region $\mathcal{U}_3$ entirely inside $\mathcal{U}_2$, i.e. $\mathcal{U}_3 \subset (\mathcal{U}_2 - {\mathcal{U}_2}^*)$, and a point $\boldsymbol{p_3}$ in its integrated stable subspaces $ISS(\mathcal{U}_3)$ such that a state trajectory passing through $\boldsymbol{p_2}$ will arrive on $\boldsymbol{p_3}$ under the system dynamics of $\dot{\boldsymbol{x}} = f(\boldsymbol{x}, \boldsymbol{u_1})$. In mathematics:

$\forall p_2 \in ISS(\mathcal{U}_2) : \exists u_1 \in \mathcal{U}_1 \ \& \ \mathcal{U}_3 \subset (\mathcal{U}_2 - {\mathcal{U}_2}^*) \ \& \ p_3 \in ISS(\mathcal{U}_3)$ such that $\exists t_2 > t_1 : x(t_2) = p_3$ under the dynamics of $\dot{x} = f(x, u_1), x(t_1) = p_2$, where $\mathcal{U}_2 \subset (\mathcal{U}_1 - {\mathcal{U}_1}^*)$ and $\mathcal{U}_2 \neq \{0\}$.

Proof:

From the definition of ISS we know that if $p_2 \in ISS(\mathcal{U}_2) \Longrightarrow \exists u_2 \in {\mathcal{U}_2}^*$ such that $p_2 \in SS(u_2) \Longrightarrow \dot{x}(p_2, u_2)$ is tangent to $ISS(\mathcal{U}_2)$.

$$\dot{x}(p_2, u) = \dot{x}(p_2, u_2) + \frac{\partial f(x,u)}{\partial u}|_{(p_2,u_2)}(u - u_2) + \cdots$$

$$\left.\begin{matrix} M(q)\ddot{q} = C(q,\dot{q}) + G(q) + u \\ \dot{x} = \begin{bmatrix}\dot{q}\\ \ddot{q}\end{bmatrix} = f(x,u) \end{matrix}\right\} \Longrightarrow \frac{\partial f(x,u)}{\partial u}|_{(p_2,u_2)} = \begin{bmatrix} 0 \\ M^{-1}(p_2)\end{bmatrix} \Longrightarrow \dot{x}(p_2,u) \cong \dot{x}(p_2,u_2) + \begin{bmatrix} 0 \\ M^{-1}(p_2)(u-u_2)\end{bmatrix}$$

Let $\hat{n}_{2m\times 1}$ be the unit normal outward vector of $ISS(\mathcal{U}_2)$ at p_2. $\hat{n}$ is perpendicular to $\dot{x}(p_2, u_2)$: $\hat{n}.\ \dot{x}(p_2, u_2) = 0$. Let's decompose $\hat{n}$ as $\hat{n} = \begin{bmatrix}[\hat{n}_1]_{m\times 1} \\ [\hat{n}_2]_{m\times 1}\end{bmatrix}$. Therefore

$$\hat{n}.\ \dot{x}(p_2, u) = \hat{n}.\begin{bmatrix} 0 \\ M^{-1}(p_2)(u-u_2)\end{bmatrix} = \hat{n}_2.M^{-1}(p_2)(u-u_2)$$

Define the ε-neighborhood of $\mathcal{U}_2$ as: $\mathcal{U}_2^{\varepsilon} = \{u \in \mathbb{R}^m | norm(u - u_2) < \varepsilon;\ \forall u_2 \in \mathcal{U}_2\}$. For a $u_2 \in \mathcal{U}_2$ vector $(u - u_2)$ covers all directions in $\mathbb{R}^m$ for $u \in \mathcal{U}_2^{\varepsilon}$, and hence $M^{-1}(p_2)(u - u_2)$ covers all directions in $\mathbb{R}^m$ as well since M is the symmetric matrix of inertia, positive definite and full rank. Thus, $\exists u_1 \in \mathcal{U}_2^{\varepsilon}$ such that $\hat{n}.\dot{x}(p_2, u_1) = \hat{n}_2.M^{-1}(p_2)(u_1 - u_2) < 0$ which means $\dot{x}(p_2, u_1)$ goes inside $iISS(\mathcal{U}_2)$. The above holds

for any $\varepsilon > 0$, implying that at a point p_2 on $ISS(\mathcal{U}_2)$ there exist a control input $u_1 \in \mathcal{U}_2^{\varepsilon} \subset \mathcal{U}_1$ which pushes the state in $iISS(\mathcal{U}_2)$, or to ISS of some $\mathcal{U}_3 \subset (\mathcal{U}_2 - \mathcal{U}_2{}^*)$. ***

This theorem says that for a certain input constraint $\mathcal{U}$, the system will be able to drive any point on the ISS of some subset of $\mathcal{U}$ - except the origin of the state space - to the ISS of some subset of that subset which will easily conclude to the balanceability of $iISS$ by using the Lyapunov 2nd theorem or the Krasovskii-LaSalle principle: the volume of the *iISS* of $\mathcal{U}$ or its current subset is always positive and can be continuously decreased except when it reaches $\{0\}$ where the algorithm stops, thus $iISS$ goes to $\{0\}$ as time goes to infinity.

For any given input constraint its $iISS$ is entirely balanceable. The input constraint in this study may be any closed subspace of which includes the origin, and is not limited to those which may appear in practice for real cases. It is not guaranteed that for any arbitrary form of the input region in the input space its $iISS$ covers the entire balanceable region. However, the following theorem gives a criterion to check whether $iISS$ of a given $\mathcal{U}$ covers the balanceable region entirely or not:

Theorem 3: For the system $\dot{\boldsymbol{x}} = f(\boldsymbol{x}, \boldsymbol{u}); \boldsymbol{u} \in \mathcal{U}$ let $\mathcal{B}(\mathcal{U})$ be the complete balanceable region. If at some time, the state of the system $\boldsymbol{x_1}$ be on the boundary of the balanceable region $\mathcal{B}^*(\mathcal{U})$, it may easily be proven that there is no possibility for the system to drive its state inside $\mathcal{B}$ (i.e. in $\mathcal{B} - \mathcal{B}^*$):

If $x_1 \in \mathcal{B}^*(\mathcal{U}) \Longrightarrow \nexists\, u_1 \in \mathcal{U}$ such that $\dot{x}(x_1, u_1)$ goes inside $\mathcal{B}(\mathcal{U}) - \mathcal{B}^*(\mathcal{U})$.

Proof (by contradiction):

Suppose that $\exists p \in \mathcal{B}^*$, $u_1 \in \mathcal{U}$ and $\Delta t > 0$ such that $(p + \dot{x}(p, u_1)\delta t) \in (\mathcal{B} - \mathcal{B}^*)$; $\forall \delta t \in (0, \Delta t]$. Suppose that Δt is very small.

Let $p_1 = p + \dot{x}(p, u_1)\Delta t$, $p' = p - \alpha \dot{x}(p, u_1)\Delta t$ where $\alpha > 0$, $p_2 = p' + \dot{x}(p, u_1)\Delta t$, and $p_3 = p' + \dot{x}(p', u_1)\Delta t$. Let d be the minimum distance from p_1 to $\mathcal{B}^*$.

$$p_3 - p_1 = p' - p + (\dot{x}(p', u_1) - \dot{x}(p, u_1))\Delta t = p' - p + \frac{\partial \dot{x}}{\partial x}|_{(p,u_1)}(p' - p)\Delta t$$
$$= -\alpha\left(1 + \frac{\partial \dot{x}}{\partial x}|_{(p,u_1)}\Delta t\right)\dot{x}(p, u_1)\Delta t$$

Therefore:

$\alpha < \frac{d}{\left\|\left(1+\frac{\partial \dot{x}}{\partial x}|_{(p,u_1)}\Delta t\right)\dot{x}(p,u_1)\Delta t\right\|} \Longrightarrow \|p_3 - p_1\| < d$ which means $p_3 \in (\mathcal{B} - \mathcal{B}^*)$ which means p' is balanceable, but it is out of $\mathcal{B}^* \Longrightarrow$ contradiction. ***

In other words, at $\mathcal{B}^*$ the state time-derivative vector $f(\boldsymbol{x}, \boldsymbol{u})$ must be outward or tangent to $\mathcal{B}^*$. This criterion may be easily checked for the boundary of a candidate for the balanceable region such as $iISS$. Furthermore, for some candidate of the balanceable

region which is entirely balanceable such as the $iISS$, if at some $\boldsymbol{x_1}$ on its boundary and some $\boldsymbol{u_1} \in \mathcal{U}$ the above condition doesn't hold, a corrective computer algorithm may extend the candidate region in the direction of $-f(\boldsymbol{x_1}, \boldsymbol{u_1})$ in order to include the missed balanceable states.

3.5. Application of the method on two mechanical models

This section will illustrate how the balanceable region, or the feasible movement area for the control of balance, can be found using the above theory. The mechanical models to be used here are planar 2-segment and 3-segment models of the human standing balance in the sagittal plane, although the methodology is the same in frontal plane for medio-lateral movements.

3.5.1. Two-segment model

Consider a well-known 2-segment mechanical model of a body in upright balance, which has been introduced in section 2.2. It consists of 1) feet, and 2) the rest of body with only one degree of freedom in its ankle joint.

The motion state of this model may be expressed by either of the ankle angle and angular velocity: $\boldsymbol{x} = [\theta \quad \omega]^T$ ($\omega = \dot{\theta}$) or by the location of the vertical projection of the CoM and its time derivative: $\boldsymbol{z} = [d \quad v]^T$, where $v = \dot{d}$. The only control input (u) to this model is the ankle torque (T_{Ankle}) by which the individual controls its state. The ankle torque is restricted to some maximum value in the dorsiflexion direction ($u_{DF_{max}}$) and some maximum value in the plantar flexion direction ($u_{PF_{max}}$). The feasible range of u, hence, is $\mathcal{U} = \{u | u_{DF_{max}} \leq u \leq u_{PF_{max}}\}$, the boundary of which consists of two points: $\mathcal{U}^* = \{u_{DF_{max}}, u_{PF_{max}}\}$. The equation of state (2-5-2) may be written as

$$\dot{\boldsymbol{x}}(t) = \begin{bmatrix} x_2(t) \\ a\sin x_1(t) + bu(t) \end{bmatrix}; \boldsymbol{x}(0) = \boldsymbol{x_0} \quad \text{(3-8)}$$

where $\boldsymbol{x_0}$ is the initial state, constants a and b are $m_B l_{B_{cm}} g / I_{Ankle}$ and $1/I_{Ankle}$, respectively. $I_{Ankle} = \bar{I}_B + m_B {l_{B_{cm}}}^2$ where $\bar{I}_B$ is the body moment of inertia about its CoM.

To find $SS(u_{PF_{max}})$, the stable subspace corresponding to $u \equiv u_{PF_{max}}$, i.e. the sort of initial states which automatically travel to some equilibrium point $\boldsymbol{x_{eq}}$ under the system dynamics of $\dot{\boldsymbol{x}}(t) = f(\boldsymbol{x}(t), u_{PF_{max}})$, the equilibrium point $\boldsymbol{x_{eq}}(u_{PF_{max}})$ must be found first, then the state trajectory passing through that point must be figured out. At an equilibrium point the state remains constant ($\dot{\boldsymbol{x}} = 0$):

$$f(\boldsymbol{x_{eq}}, u_{PF_{max}}) = 0 \Rightarrow \boldsymbol{x_{eq}} = \begin{bmatrix} \sin^{-1}\left(-\frac{b}{a} u_{PF_{max}}\right) & 0 \end{bmatrix}^T \quad \text{(3-9)}$$

The state trajectory passing through this point for the input $u = u_{PF_{max}}$ may be found as

$$x_2{}^2(t) = -2a\left(\cos x_1(t) - \cos\left(\sin^{-1}\left(-\frac{b}{a}u_{PF_{max}}\right)\right)\right) + 2bu_{PF_{max}}\left(x_1(t) - \left(\sin^{-1}\left(-\frac{b}{a}u_{PF_{max}}\right)\right)\right);\ \ x_2(t) \neq 0 \quad (3\text{-}10)$$

Eq. (3-10) produces four curves, two of which align with the stable eigenvector and show the stable subspace of system (3-8) with $u \equiv u_{PF_{max}}$. The other stable subspace, $SS\left(u_{DF_{max}}\right)$, can be found in a similar way.

In order to produce numerical results, average anatomical values (Winter, 2009) are used, as shown in Table 3-1, which are similar to those used in Pai & Patton (1997) and Hof et al., (2005). The control input constraint is set to $u \in \mathcal{U} = [-167.0 \sim +39.17]$ (+: dorsiflexion) which closely simulates the conditions in those studies. The stable subspaces for such a model are shown in Figure 3-7-a: the green curve= $SS(+39.17)$ and the red curve= $SS(-167.0)$, inside which is $iISS(\mathcal{U})$ which is proven to be balanceable . Theorem 3 helps to make sure that $iISS$ covers the balanceable region of system (3-8) entirely. At $\boldsymbol{x_1} = [0.439 - 0.676]^T$ on $SS(-167.0)$ (thus on $ISS(\mathcal{U})$), for example, the direction of $f(\boldsymbol{x_1}, u)$ for all $u \in \mathcal{U}$ is drawn in Figure 3-7-a, in the upper right corner. It shows there is no possibility to enter the ISS at $\boldsymbol{x_1}$ if constrained to inputs within $\mathcal{U}$, since all the trajectories at this point are tangent to or outward of ISS. Checking the criterion of Theorem 3 for all points on ISS confirms that there is no balanceable point on ISS or outside it, and hence, that $iISS(\mathcal{U})$ is exactly and thoroughly the $\mathcal{B}(\mathcal{U})$ since a trajectory from outside ISS to the origin will surely cut through ISS.

Table 3-1. Anatomical parameters used for the 3-link model of section 2.3.

Body	Mass	$m_B = 72.825\ kg$
	Moment of inertia (CoM)	$\bar{I}_B = 11.7057\ kg.m^2$
	Hip to CoM length	$l_{B_{CM}} = 0.8755\ m$
Feet	Mass	$m_F = 2.175\ kg$
	Length, toe to heel	$l_f = 0.2660\ m$
	Height, ground to ankle	$y_A = 0.0683\ m$
	Toe to ankle (horizontal)	$x_A = 0.2155\ m$
	Toe to CoM (horizontal)	$x_{f_{CM}} = 0.1330\ m$

The balanceable region in the $\boldsymbol{x}$-plane may be mapped into the $\boldsymbol{z}$-plane by

$$\begin{aligned} d &= \left(x_A - l_{B_{cm}}\sin(\theta)\right)/l_F \\ v &= \left(-l_{B_{cm}}\dot{\theta}\cos(\theta)\right)/H \end{aligned} \quad (3\text{-}11)$$

where $\boldsymbol{z} = [d \quad v]^T$, d and v are the horizontal location of the CoM normalized to the feet length and the horizontal velocity of the CoM normalized to the body height. The balanceable region found above transferred into the $\boldsymbol{z}$-plane as well as those proposed in Pai & Patton (1997) and in Hof et al., (2005) are shown in Figure 3-7-b.

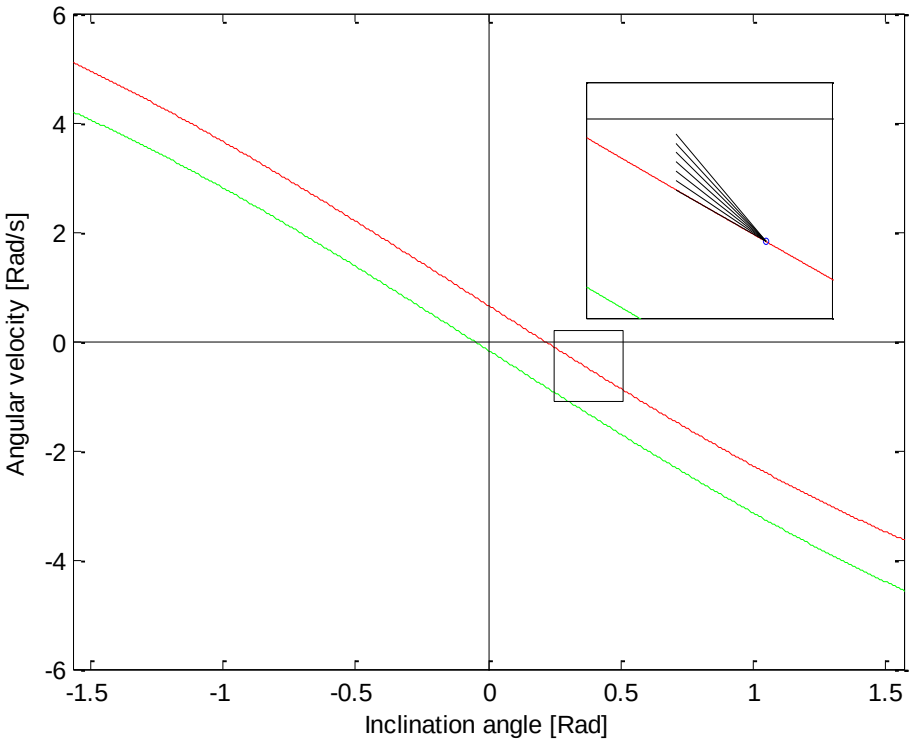

a)

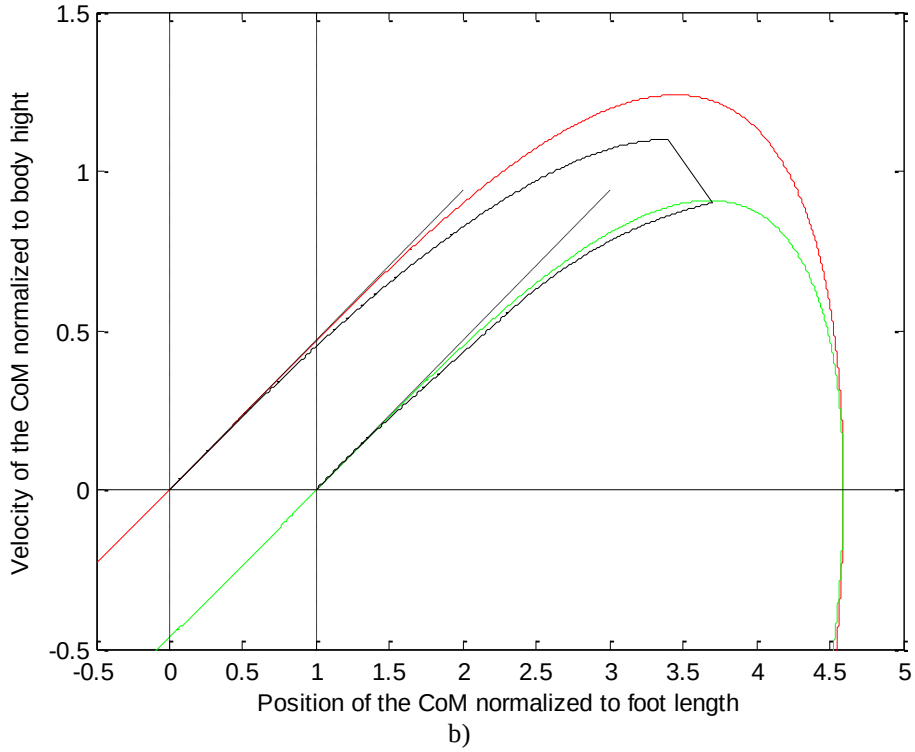

b)

Figure 3-7. a) Stable subspaces corresponding to the maximum torque in dorsiflexion (green curve) and plantar flexion (red curve) directions, in the angle-angular velocity ($\boldsymbol{X}$) plane. The area between the two curves is balanceable. The criterion of Theorem 3 is checked and confirmed. As an example, $f(\boldsymbol{x}, \boldsymbol{u})$ at one state $\boldsymbol{x} = [0.439 - 0.676]^T$ for all $u \in \mathcal{U}$ is shown. b) Boundaries of the balanceable region mapped in the $\boldsymbol{z}$-plane (green and red curves), and those obtained in Pai & Patton (1997) (solid black) and in Hof et al. (2005) (dash-dotted black).

The main two boundaries of the balanceable region found by the method of this research match those of Pai & Patton (1997). However, we have missed a third boundary which comes from a condition on the exerted torque on the ankle joint in large movements in order to ensure that the pressure-type nature of the GRF holds. Such a condition cannot be seen in the form of the control input constraint considered in this study. A discussion on the input constraints will be done later.

3.5.2. Three-segment model

In this section we will apply the same theory on a more complicated model as well, in order to figure out its balanceable region. Consider a 3-segment mechanical model which has been introduced in section 2.3, consisting of 1) feet, 2) lower limbs (excluding the feet), and 3) the upper body, jointed at the ankle and hip with the sagittal symmetry is assumed. Two degrees of freedom for this model are rotations in ankle and hip joints.

A set of four variables is needed to express the state of this model, e.g. $\boldsymbol{x} = [\theta_1 \quad \theta_2 \quad \dot{\theta}_1 \quad \dot{\theta}_2]^T \in \mathbb{R}^4$ where θ_1 and θ_2 are the lower limbs and upper body inclination angles respectively, and $\dot{\theta}_1$ and $\dot{\theta}_2$ are their time-derivatives.

The control input vector u consists of the ankle and hip torques: $\boldsymbol{u} = [T_{Ankle} \quad T_{Hip}]^T$, which is restricted to some region in the input space: $\boldsymbol{u} \in \mathcal{U} \subset \mathbb{R}^2$. For an input $\boldsymbol{u}^*$ on $\mathcal{U}^*$ the equilibrium state of the system $\dot{\boldsymbol{x}} = f(\boldsymbol{x}, \boldsymbol{u}^*)$ is

$$\boldsymbol{x_{eq}}(\boldsymbol{u}^*) = \left[\sin^{-1}\left(\frac{-{u_A}^*}{g\left(m_L l_{L_{CM}} + m_H l_{L_H}\right)}\right) \quad \sin^{-1}\left(\frac{-{u_H}^*}{g m_H l_{H_{CM}}}\right) \quad 0 \quad 0\right]^T \quad (3\text{-}12)$$

The stable subspace for this system near its equilibrium point is the span of the stable eigenvectors of the linearized matrix $\boldsymbol{A}$:

$$\boldsymbol{A} = \frac{\partial f(\boldsymbol{x}, \boldsymbol{u}^*)}{\partial \boldsymbol{x}}\Big|_{\boldsymbol{x}=\boldsymbol{x_{eq}}} = \begin{bmatrix} \frac{\partial f_1}{\partial x_1} & \cdots & \frac{\partial f_1}{\partial x_4} \\ \vdots & \ddots & \vdots \\ \frac{\partial f_4}{\partial x_1} & \cdots & \frac{\partial f_4}{\partial x_4} \end{bmatrix} \quad (3\text{-}13)$$

which is a 2-dimensional plane. To obtain the $SS(\boldsymbol{u}^*)$ entirely, one may solve the state trajectories that pass through points on the stable subspace near the x_{eq}, i.e. solve the system $\dot{x} = f(x, u^*); x(0) = x_0$ with negative time steps, where $x_0 = c_1\boldsymbol{v_1} + c_2\boldsymbol{v_2}$, $\boldsymbol{v_1}$ and $\boldsymbol{v_2}$ are the stable eigenvectors of $\boldsymbol{A}$, c_1 and c_2 are arbitrary real values, such that ${c_1}^2 + {c_2}^2$ be very small. $ISS(\mathcal{U})$ is the set of all $SS(\boldsymbol{u}^*)$ for all $\boldsymbol{u}^* \in \mathcal{U}^*$ and is a 3-dimensional surface separating $iISS$ from $oISS$ in the 4-dimensional state space.

Average anatomical values of Table 3-2 (Winter, 2009) and a rectangular shape of the feasible input region are used as

$$\mathcal{U} = \left\{ \begin{bmatrix} u_A \\ u_H \end{bmatrix} | u_{A_{min}} \le u_A \le u_{A_{max}} \,\&\, u_{H_{min}} \le u_H \le u_{H_{max}} \right\}$$

Table 3-2. Anatomical parameters used for the 3-link model of in section 2.2.

HAT	Mass	$m_H = 50.85\ kg$
	Moment of inertia (CoM)	$\bar{I}_H = 3.1777\ kg.m^2$
	Hip to CoM length	$l_{H_{CM}} = 0.1885\ m$
Lower Limbs	Mass	$m_L = 21.975\ kg$
	Moment of inertia (CoM)	$\bar{I}_L = 1.5489\ kg.m^2$
	Ankle to CoM length	$l_{L_{CM}} = 0.5637\ m$
	Ankle to hip length	$l_{L_H} = 0.8592\ m$
Feet	Mass	$m_F = 2.175\ kg$
	Length, toe to heel	$l_f = 0.2660\ m$
	Height, ground to ankle	$y_A = 0.0683\ m$
	Toe to ankle (horizontal)	$x_A = 0.2155\ m$
	Toe to CoM (horizontal)	$x_{f_{CM}} = 0.1330\ m$

with $u_{A_{min}} = -167.0$, $u_{A_{max}} = +39.17$, $u_{H_{min}} = -87.85$, and $u_{H_{max}} = +102.0$ (Figure 3-8) and the ISS was obtained for this system. Figure 3-9 shows the part of the balanceable region which has zero angular velocities (a), the part with zero angles (b), and the part in which $\theta_1 = \theta_2$ & $\dot{\theta}_1 = \dot{\theta}_2$ in the $\theta - \dot{\theta}$ plane (c) and in the $d - v$ plane (d). Figures c) and d) show which initial states with an aligned lower and upper body and the same angular velocities are balanceable, which is generally similar to the balanceable region of Figure 3-7. This is because the dynamics of the two and three-segment models are not so different in configurations determined by the condition of $\theta_1 = \theta_2$ & $\dot{\theta}_1 = \dot{\theta}_2$, since the third link's length ($l_{H_{CM}}$) is small. Minor differences mainly come from 1) Hip bending, which makes the 3-segement model more capable in momentum management, and explains the upper shifting of the upper boundary. Therefore, the area between the upper blue curve and upper solid black curve in Figure 3-9-d which has been declared not balanceable by a 2-segment model is now found balanceable by a 3-segment model including a hip joint. 2) The torque limit on the hip joint of the 3-segement model which prevents the application of torques big enough in states bellow the lower blue curve, while such a limitation doesn't exist in the 2-segment model. Thus, there is an area in Figure 3-9-d which is balanceable according to the 2-segment model and not according to the 3-segment model.

However, it should be noted that Figure 3-9-d shows only a cross-section of the balanceable region for the 3-segment model, not the projection of the balanceable region in z-plane. Many body configurations (states) in the 4-dimensional state space of the 3-segment model, including both balanceable and non-balanceable points, would be mapped into the same point in posidion-velocity of the CoM plane (z-plane). This means that the range of feasible movements for the control of balance in a 3-segment model cannot be thoroughly compared by areas in the z-plane. A seperate study may focus on a thorough analysis and comparison of the results from different models, e.g. to consider how the feasible range of movements vary when shifting from ankle strategy to hip or squat strategies.

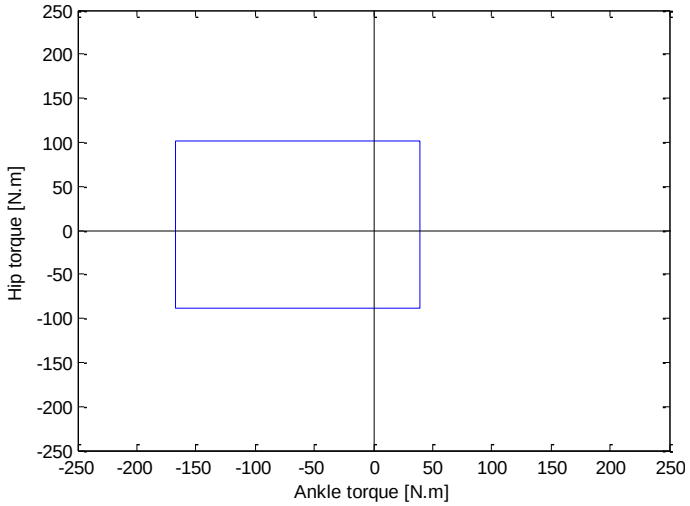

Figure 3-8. The control input constraint used in section 3.5.2. The input (ankle and hip torque) may take values only from inside the blue rectangle. It is also called the feasible input region.

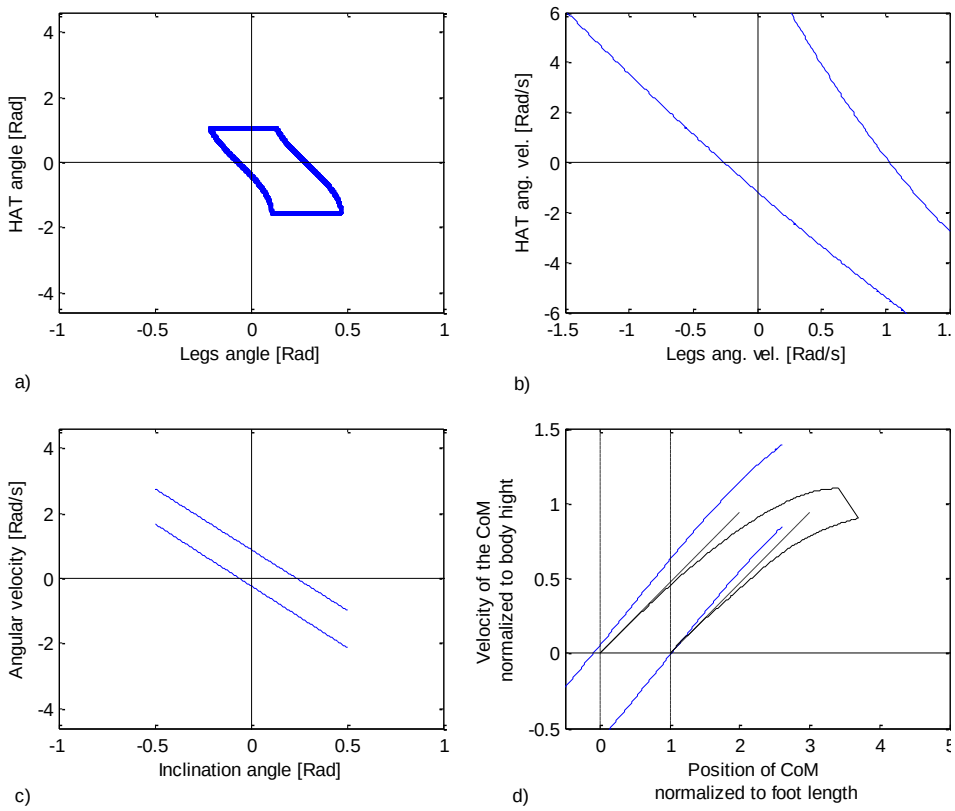

Figure 3-9. Some aspects of the balanceable region in the 4-dimensional state space: the part with zero Legs and HAT angular velocity (a), with zero angles (b), with equal angles and equal angular velocities (c). d) Figure (c) mapped into the $\boldsymbol{z}$-plane (blue curves) and the balanceable region obtained in Pai & Patton (1997) (solid black) and in Hof et al. (2005) (dashed black).

Boundaries in Figure 3-9 are not so smooth, which should be related to the low resolution of the 4-dimensional matrix that stores the ISS. Increasing the resolution would increase the matrix size by a fourth power.

3.6. Discussion

3.6.1. The Control Input Constraint

The less restricted the joint torques are, the larger the balanceable region is. The motor (muscle) maximum force (active+passive), geometry of the joint (the point of action of forces, muscle directions, the instantaneous center of rotation), and the mechanical strength of tissues engaged in force transmission and joint stability (bones and soft tissues), restrict the possible joint torques. For example, the average (standard deviation) isometric maximum ankle torque for both legs together in dorsiflexion and plantar flexion and hip torque in flexion and extension are reported to be 47.44 (14.58) and 90.70 (56.24), 191.09 (56.24), and 87.85 (73.41) Newton-meters, respectively, for a group of about 1000 Japanese adults (NITE, 2003). The actual values vary with each subject. However, the maximum motor torque is not the only constraint. Foot-ground contact conditions (the vertical component of the contact force must be in pressure form, its horizontal component must comply with static friction requirements, location of the CoP is limited) also have to be satisfied. For example, for a foot length of $27.1\mathrm{cm}$, the ankle to toe horizontal distance of $21.9\mathrm{cm}$, and the body mass of $80\mathrm{kg}$, the dorsiflexor torque on ankles may not exceed $39.17\mathrm{N.m}$, which is less than the dorsiflexor torque most of the people are able to produce in their ankles.

The maximum torque an individual is able to produce in a joint varies with the joint angle as well as its angular velocity, since joint geometry and muscle forces are position/velocity dependent. In addition, the limit of applicable joint torques in order to maintain the stability conditions and keep the feet stationary on the ground varies with the kinematics and dynamics of the entire body. The control input constraint, therefore, is state-dependent in reality, while in this study state-invariant input constraints were used for simplicity. However, the results may be extended easily to the state-variant input regions by localizing the ISS for each state.

The control input an individual actually applies in response to a sudden balance perturbation in order to prevent a fall from initiating may be less than what they are mechanically able to exert. Non-mechanical factors will be involved as well, such as acute or chronic pain (Farina et al., 2004) and fatigue (see e.g. Beelen & Sargeant, 1991; Spendiff et al., 2002), which means a perturbation might lead to a fall for an individual, though he is mechanically able to recover its balance. Nevertheless, this research doesn't focus on how to find the control input constraint for an individual. The method of this research works for all closed feasible input regions (origin must be included) of any shape.

3.6.2. Existence of Stable Subspaces

The range of feasible movements of a body for the control of balance with certain constraints is figured out in this research by some particular state trajectories (stable subspaces) corresponding to the boundary of torque constraints. Each of such trajectories meets the equilibrium point corresponding to one of the points on the boundary of the

input torque constraints, under the system dynamics with that certain input. However, the existence of an equilibrium point for an arbitrary input torque is not proven. A question arises here: how to find the balanceable region if no stable subspace exists for some inputs? In fact, such a condition may happen for the shoulder joint, knee, and even the hip joint. The answer is, for a control input on the boundary of the input constraint and with no corresponding stable subspace, the *extreme* trajectory should be used instead which satisfies all the constraints and meets the stable subspace of another control input which has an equilibrium point in the feasible input region, inside the feasible input region. An extreme trajectory is that, if it is selected, all other trajectories of the above condition for the same system dynamics will be included in $iISS$. To illustrate, let's turn back to the 2-segment model. From equation (5) the condition for the existence of the stable subspace for a control input u is

$$-\frac{a}{b} \leq u \leq \frac{a}{b} \quad (10)$$

which is $-779.9 \leq u \leq +779.9$ for anatomical values of table 1. The control input constraint used in section 3.1 pretty well satisfies the existence condition entirely, i.e. for all the torques in the assumed feasible input range stable subspaces exist. Now, in order to demonstrate how to deal with a case in which an equilibrium point is missing, and in order to avoid complexities in explanation and demonstration for a more degrees of freedom model, let the input constraint for the same 2-link model be the very unrealistic range of

$$\mathcal{U} = \{u| -500 \leq u \leq +1000\}$$

such that includes inputs with no stable subspace. Also, suppose that a state may excurse inside the window of $\mathcal{X} = \{\boldsymbol{x} \in \mathbb{R}^2 || \boldsymbol{x_1}| \leq 1\}$ only, i.e. $-60^\circ \leq \theta \leq +60^\circ$, otherwise the system has failed to control its balance.

Stable subspaces for all control inputs for which a stable subspace exists are shown in Figure 3-10: the red curves. For $u^*{}_1 = -500\text{N.m}$ on the boundary of $\mathcal{U}$, the equilibrium point $\boldsymbol{x_{eq}} = [-0.70 \quad 0]^T \in \mathcal{X}$, and therefore $T_1 = \{\boldsymbol{x} \in \mathbb{R}^2 | \boldsymbol{x} \in \mathcal{X}, \boldsymbol{x} \in SS(u^*)\}$ forms the upper part of the ISS (thick red curve). The input $u^*{}_2 = +1000\text{N.m}$ on the boundary of $\mathcal{U}$ doesn't satisfy the condition (10) and hence, no equilibrium point exists. The extreme trajectory satisfying the system constraints should be used instead of $SS(u^*{}_2)$. All state trajectories of the system (4) with $u = +1000$ are drawn in Figure 3-10: the blue curves. The curve T_2 which passes through the point $[-1 \quad 0]^T$ is the extreme trajectory of this input and forms a part of the ISS since it is the only one that excludes no trajectory in ISS which cuts a stable subspace while satisfying the constraints. The ISS for this system is therefore, the area bounded by T_1, T_2, and $\mathcal{X}$, i.e. the four corners of which are marked with an "x" in Figure 3-10.

3.6.3. Limitations

A state-invariant input constraint was assumed in this research for simplicity. A constraint expressed in such a way cannot simulate any state-variant condition on the input torque, e.g. the condition imposed by the necessity of being the GRF always upward.

This is why the corresponding third boundary of the balanceable region couldn't be found in Figure 3-7. A future extension may consider a general form of the state-variant input constraint and figure out the balanceable region by localizing the integrated stable subspaces at every point of its boundary.

In this research, like the previous ones, the feasible range of movements for the control of balance addresses the physical feasibility for a mechanical model where the maximum torque an individual can apply on their joints as well as the anatomical parameters play the key role. The model may be extended to include the control system as well, in order to differentiate between the balanceable regions for individuals with not only different mechanics but different control skills as well. For example, adding a response delay into the model will map a state to a point in the instant response model which will be the destination of that state after the response time.

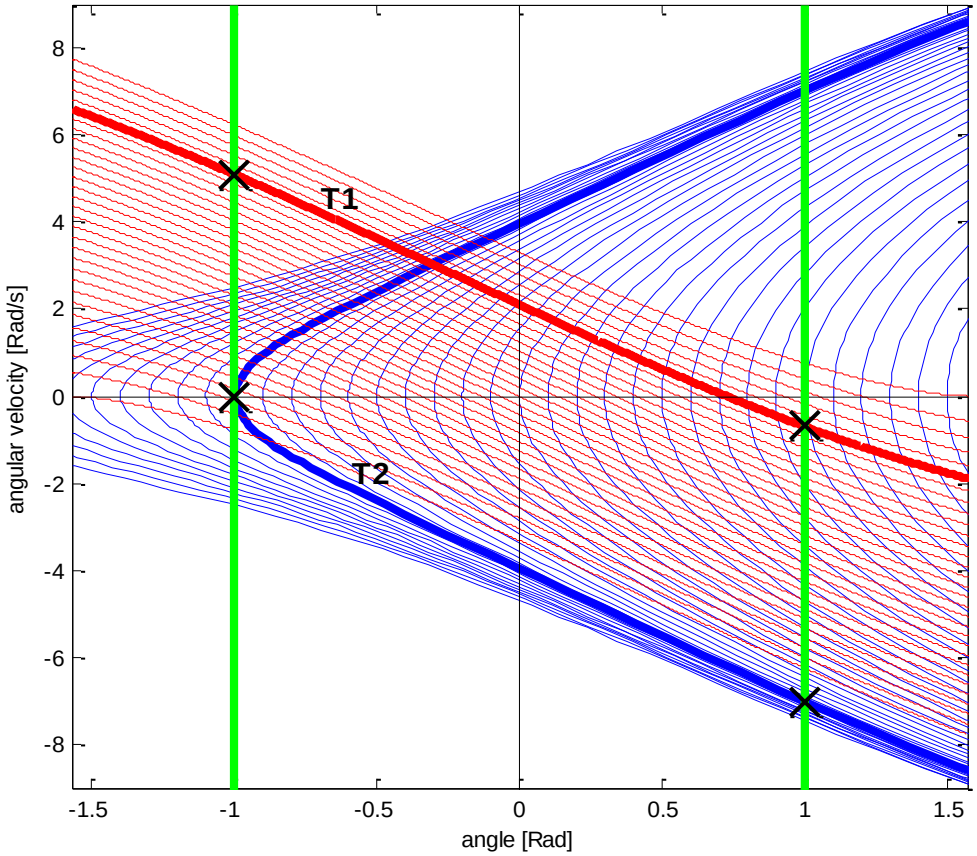

Figure 3-10. Theoretical balanceable region for an unrealistic input constraint of $-500 \leq u \leq +1000$ $[N\,m]$ to show how to deal with a case where no stable subspace exists. Red curves are stable subspaces for all the inputs for which a stable subspace exists (condition 10). $SS(-500)$ forms the upper border of the balanceable region (the thick red curve, T_1). For $u = +1000$, no stable subspace exists, and the extreme trajectory should be used instead. Blue curves are state trajectories of system (4) for $u = +1000$, and the extreme trajectory is the thick blue one (T_2). All trajectories below T_2 cannot be kept inside $\mathcal{X}$ by the system, and those above it are able to be driven to an equilibrium point, and therefore are able to be driven to the origin. Lateral boundaries are imposed by the state constraint (green lines). The balanceable region for this system is the area between the "x" marks.

3.7. Summary

In this section we addressed the question of what is the feasible range of movement for a body to remain balanced while in upright postures. A feasible region in the center of mass position-velocity plane has been proposed previously. We showed that for a certain individual with given anatomical and mechanical characteristics, the feasible movements of the CoM, or more generally the range of states at which the control of balance would be possible, can be analytically found through a mechanical reasoning. We introduced a subspace of the motion state space, namely the integrated stable subspaces (*ISS*), and proved that the control of balance is possible all over the *ISS*. In order to illustrate how the method may be used in practice, the feasible region for a well-known one-DoF mechanical model as well as for a two-DoF one is found using this approach, and is compared to that found by the conventional method. The feasible region found by this approach depends on the physical properties of a body including anatomical parameters of a body as well as the torque (control input) constraints. This method works with any arbitrary shape of the input constraint.

Chapter 4

The new metric for postural upright stability: Probability of Recovery - PoR

4.1. Introduction

Balance gets disturbed by perturbations of different types, then, escaping from the initiation of a fall the individual starts a procedure to recover balance. After a person feels at risk of the loss of balance and after some reaction delay, the recovery procedure commences and lasts until advancing the posture to a safe one. Let's call the start point of the recovery trial a "*perturbed state*", and without loss of generality, assume that the objective of recovery is to drive the posture to an exactly upright position without any part of the body moving. The balance is *recovered* if and only if this objective is achieved. The possibility of an individual to recover his or her balance from a perturbed state, in addition to the individual's characteristics, depends on the perturbed state. The more severe a perturbation is, the more recovering from the corresponding perturbed state becomes difficult, where one may say that state is far from balance, or the *postural upright stability* at that state is poor. In many cases, research or practice, it is essential to quantitatively know how good the balance is at a body posture or at every moment during a task. In this part of this research a quantitative metric to assess the upright stability at a certain state is the matter of interest

We take advantage of the idea of risk of fall initiation and suggest a new measure for the postural upright stability which assigns a value to a body state based on the probability of avoiding a fall initiation from that state. A value between 0 (highly unstable) and 1 (highly stable) is allocated to a body state describing how possible maintaining/regaining the balance is at that state. It is in close relation with how safe being in a certain state is, with respect to the loss of balance. It will be defined conceptually first, then a three-segment mechanical model will be selected as a platform based on which we will explain how it may be calculated and show some results. Results will be shown and compared for a 2-link model as well. This new measure will also be compared to the conventional metric: margin of stability (MoS).

4.2. The no-risk curve

For a free uncontrolled inverted pendulum, for every angle (θ_B), which is measured from the vertical line, between $-\pi/2$ and $\pi/2$ there exist an angular velocity ($\dot{\theta}_B$) in the opposite direction which drives the pendulum to an upright posture with zero velocity after some time.

Now, consider the 2-segment mechanical model of section 2.2. This model is slightly different than a simple inverted pendulum since we have two segments. In order for a body part to behave like a simple pendulum, constraints (2-4-1) to (2-4-3) must be satisfied. Therefore, for a subject in a situation having some (x, v) corresponding to the above mentioned pair of $(\theta_B, \dot{\theta}_B)$ according to (2-7-1) and (2-7-2), it will easily be driven to a static

upright posture without any effort, if constraints (2-4-1) to (2-4-3) are satisfied during this motion. Thus, such a pair of (x, v) is a "no-risk point", since no one will initiate a fall from it. To find all no-risk points, one may set $u \equiv 0, \forall t$ in the equation of state (2-6-2) and obtain the no-risk curve (NRC) as follows:

$$\dot{\theta}_B{}^2 = 2a(1 - \cos\theta_B) \quad (4\text{-}1)$$

where $a = \frac{m_B l_{B_{CM}}}{\left(\bar{I}_B + m_B l_{B_{CM}}{}^2\right)} g$. Rewriting (4-1) for x and v delivers

$$v^2 = \frac{2m_B g}{\left(\bar{I}_B + m_B l_{B_{CM}}{}^2\right)} \left(l_{B_{cm}} - \sqrt{l_{B_{cm}}{}^2 - (x_A - x)^2} \right) \left(l_{B_{cm}}{}^2 - (x_A - x)^2 \right) \quad (4\text{-}2)$$

In order to get rid of individual's characteristics and obtain general results, we use normalized position and velocity of the body CoM as defined in (2-8-1) and (2-8-2). Thus, the equation of the NRC will become as

$$\bar{v}^2 = \frac{2}{1 + \left(\frac{l_{B_g}}{l_{B_{cm}}}\right)^2} \left(1 - \sqrt{1 - \bar{x}^2}\right)(1 - \bar{x}^2) \quad (4\text{-}3)$$

where l_{B_g} is the gyration radius of the body ($\bar{I}_B = m_B l_{B_g}{}^2$). According to anthropometric databases (for ex. see Winter, 2009) $l_{B_g}/l_{B_{cm}}$ may be estimated as 0.4579. The dashed red curve in Figure 4-1 shows the NRC in Y-plane. For example, for the CoM to be behind the ankle at 0.25 times of its distance to the ankle (which is, for an average male, about $22\ cm$), a normalized forward velocity of 0.2204 (which about $0.65\ m/s$ for an average male) is needed to drive it to exactly above the ankle and stop it, in the absence of any ankle torque.

However, equation (4-3) for the no-risk curve is obtained under the assumption of an absence of any control input, i.e. ankle torque, always, for every body state. In the reality the control input is a summation of active and passive torques, i.e.

$$u(t) = T_{ac}(t) + T_{ps}(t) \quad (4\text{-}4)$$

where T_{ac} and T_{ps} are the active and passive ankle torques [*N.m*], respectively. In reality, what every person with any level of strength may apply is a zero *active* torque, and since a passive moment might exist depending on the posture, the control input will not be always zero. Passive torque-angle relationship has been modeled by exponential summations as follows:

$$T_{ps}(\theta_B) = B_1 e^{k_1 \theta_B} + B_2 e^{k_2 \theta_B} \quad (4\text{-}5)$$

where B_1, B_2, k_1, and k_2 are coefficients obtained by experiments. Values obtained for a group of male adults aged over 65 years old are 5.693E-5, -0.488, -21.088, and 7.309 respectively (Anderson et al., 2007). By adding a small constant value to the passive torque-angle relation (4-5), one may remove its bias in order to have $T_{ps}(0) = 0$.

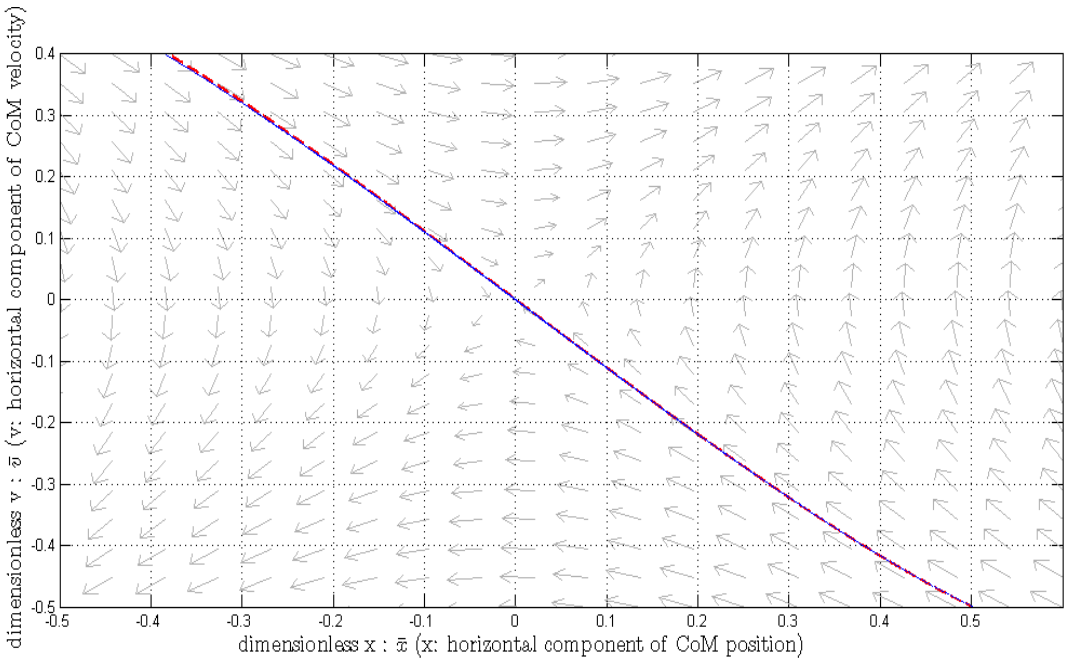

Figure 4-1. No-risk curve (NRC), assuming zero input, i.e. passive torque is assumed not dependent to angle (dashed red curve), and without the above assumption, i.e. torque varies with angle (solid blue curve). Axes are horizontal position and horizontal velocity of the body center of mass normalized by equation (2-8-1) and (2-8-2). Origin ($\bar{\boldsymbol{x}} = \bar{\boldsymbol{v}} = \mathbf{0}$) corresponds to the static upright posture. Arrows correspond to dynamic traces for the zero-input case, showing that without making any efforts the system will get far from the balance when concluding with a fall, for all initial conditions except those lying on the no-risk curve.

NRC in this case, i.e. without the assumption of zero passive torque for all angles, can be calculated through an easy numeric method. Set the active torque to zero for all times ($T_{ac} = 0, \forall t$), and the control input at a given state will be the passive torque at that state:

$$(4\text{-}4) \Rightarrow u(x, v) = T_{ps}\big(\theta_B(x)\big)$$

By substituting this input in the equation of state (2-6-2) and solving it with a negative time step, the no-risk curve can be found. It is shown in Figure 4-1. A remark here is, if the solver starts at the origin of the $x - v$ plane, which corresponds to an upright posture without motion, the equation of state delivers the trivial solution of $x \equiv v \equiv 0$. To avoid this problem, the solver should start with some initial states on the curve of (4-3) and very close to the origin, since for points close to the origin of $x - v$ plane $T_{ps}(x) \approx 0$ and thus equation (4-3) works. As shown in Figure 4-1, the no-risk curves obtained with and without the simplifying assumption of zero passive torque almost overlap, except at the two ends where small differences can be seen. For the same example of $\bar{x} = -0.25$ the necessary normalized velocity is found to be $\bar{v} = 0.2219$ which is only 0.7% different from the previous result (0.2204).

4.3. The new metric for upright balance: conceptual definition

The term "state" is used in this work to describe the body situation at a moment which may be expressed by a vector consisting of all postural and movement variables, e.g. joint angles and angular velocities. State space is then a virtual n-dimensional space (n: the number of state variables), each axis of which is one of the joint angles or angular velocities. Any human movement, like balance recovery trial, may be described by a curve in the state space, showing what the body state is at any point in time.

Postural stability is different from state to state. At the body states on the so called no-risk curve everybody are able to control their balance, since no active action is needed at those situation, and everybody have the ability to accomplish the no action job. At some other body states (e.g. CoM behind the BoS with a backward velocity) no one is able to maintain its balance and a fall will surely initiate. Thus, the postural stability at these situations is poor. A postural stability value should be assigned to every state to show how good the balance is at each state.

For points other than those on the NRC, without making some efforts a subject will undoubtedly initiate a fall (see the phase plane shown in Figure 4-1). To avoid beginning a fall a subject must make some efforts. Even under a perfect reaction, some subjects will be successful and the others will lose their balance, depending on their strength. The portion of fallers varies from state to state. One may argue that a bigger stability value should be granted to the state from which a smaller portion of the society will initiate a fall, which directly implies how safe that state is. This is the key idea behind our new stability metric. By using the population's statistical characteristics and taking advantage of the concept of probability, the postural stability at a state may be defined as the probability of the balance to be recoverable from that state over the entire population, without initiation of a fall, and called the *probability of recovery (PoR)*.

4.4. How to calculate PoR

PoR, may be solved on any mechanical model, whether planar or spatial, both legs paired with sagittal symmetry or independent legs, and any number of segments. Nevertheless the complexity of the model dramatically increases the computation burden. In order to define this new stability measure in more details and illustrate how it will be found for a state we use a simple yet most common mechanical model in the balance analysis research as a chassis, although the methodology may be extended to other mechanical models.

4.4.1. Dynamic model

The model is a 2-segment linkage introduced in section 2.2. Using such a sagittal model, an individual's situation at a moment (state) may be expressed uniquely by a set of 2 variables: the normalized location of the vertical projection of the CoM ($\bar{x}$) and the normalized horizontal velocity of the CoM ($\bar{v}$), i.e. state can be

$$\mathrm{Y} = \begin{bmatrix} \bar{x} \\ \bar{v} \end{bmatrix}$$

or the body inclination angle (θ_B) and its angular velocity ($\dot{\theta}_B$), i.e.

$$\mathrm{X} = \begin{bmatrix} \theta_B \\ \dot{\theta_B} \end{bmatrix}$$

The equation of state for X and Y is given in equations (2-6-2) and (2-10-2), respectively. The foot constraints that restrict the applicable ankle torque are given in relationship (2-12).

The control input into this model by which the individual controls his or her posture is the ankle torque. Control input at state X is limited to a band $T_{Set}(X) = \left[T_{PF_{Max}}(X), T_{DF_{Max}}(X)\right]$ which varies with the state, but $T_{Set}(0)$ is an attribute of the individual. Abbreviations PF and DF stand for plantar flexion, and dorsiflexion respectively. For example, $T_{PF_{Max}}(0)$ is the maximum plantar flexion torque this specific person can apply on his or her ankle in a still, erect standing position.

4.4.2. The balance recovery problem

It is the problem of checking whether the control of balance at a given perturbed state X_0 is possible for a certain subject with a given $T_{Set}(0)$. With a control input trajectory (input at every point in time) candidate and a given initial state, a computer program may solve the dynamic equation (e.g. by Runge-Kutta method) and obtain the state trajectory $X(t)$. Control input trajectories will be searched on, and if there exists one such that 1) drives the body from X_0 to 0, 2) complies with the applicable input range at every state ($T_{Set}(X)$) for that specific subject, 3) all the joint angles remain within their range of motion, 4) foot constraints always hold, and 5) the movement excludes a fall, the outcome of the balance recovery problem is positive. Though several methods have been developed to find an optimal input trajectory for a movement (see e.g. Helbig et al, 1998; Atkeson & Stephens, 2007; Honarvarmahjoobin, 2009) a direct search over the possible input trajectories should be utilized since only the existence of a solution is important here.

4.4.3. Torque limits at a given state, $\boldsymbol{T_{Set}(X)}$

Both the active and passive torques vary with the joint angle and its angular velocity, since the maximum force each muscle can generate depends on the muscle length and its contraction rate, and hence depends on the joint angle and angular velocity at the time. In addition, the muscle force direction and its moment arm varies with the joint angle. Models have been generated to simulate the force-length-velocity dependency of muscles or torque-angle-angular velocity relationships for joints, based on a Hill-type model (Hill, 1938; Chow et al., 1999; King and Yeadon, 2002; Anderson et al., 2007). This study uses the model developed by Anderson et al. (2007) which suggests equation (4-5) to correlate the passive torque (T_{ps}) to the joint angle (θ), and equation (4-6) to correlate the maximum active torque (T_{ac}) to the joint angle and angular velocity ($\dot{\theta}$):

$$T_{ac}(\theta, \dot{\theta}) = \begin{cases} C_1 \cos\left(C_2(\theta - C_3)\right)\left(\frac{2C_4C_5 + \dot{\theta}(C_5 - 3C_4)}{2C_4C_5 + \dot{\theta}(2C_5 - 4C_4)}\right); \ \dot{\theta} \geq 0 \\ C_1 \cos\left(C_2(\theta - C_3)\right)\left(\frac{2C_4C_5 - \dot{\theta}(C_5 - 3C_4)}{2C_4C_5 - \dot{\theta}(2C_5 - 4C_4)}\right)\left(1 - C_6\dot{\theta}\right); \ \dot{\theta} < 0 \end{cases} \quad (4\text{-}6)$$

where $B_1, B_2, k_1, k_2, C_2, C_3, C_4, C_5$, and C_6 are correlation constants. Values obtained by Anderson et al. (2007) are given in Table 4-1. Constant C_1 equals to $T_{jnt_{max}}(0)$; $jnt =$

Table 4-1. Values of $\boldsymbol{C_2}$~$\boldsymbol{C_6}$ in torque-angle-angular velocity relationships (Equations 4-5 and 4-6), for male adults over 65yo, in plantarflexion (PF), dorsiflexion (DF), hip extension (HE), and hip flexion (HF) directions. Data from Anderson et al. (2007).

		B_1	B_2	k_1	k_2	C_2	C_3	C_4	C_5	C_6
Ankle	PF	5.693E-5	-0.488	-21.088	7.309	1.465	0.498	0.490	1.867	0.571
	DF					1.419	-0.174	0.561	1.558	1.198
Hip	HE	-2.671	0.092	-7.850	5.192	0.896	1.125	1.561	3.152	0.477
	HF					0.762	-0.269	1.875	3.819	0.296

$\{PF, DF\}$ and $T = T_{jnt_{max}}\left(\theta_{jnt}, \dot{\theta}_{joint}\right)$; $jnt = \{PF, DF\}$. As stated in equation (4-4), the applied torque on a joint is the summation of active and passive torques:

$T\left(\theta, \dot{\theta}\right) = T_{ps}(\theta) + T_{ac}(\theta, \dot{\theta})$

For example, to find the maximum active ankle torque in the plantar flexion direction, when the ankle angle is θ_A and its velocity is $\dot{\theta}_A$, substitute $C_1 = T_{PF\,Max}(0)$ in equation (4-6) (since $T_{ps}(0) \approx 0$) and find $T_{ac}(\theta_A, \dot{\theta}_A)$. This added to $T_{ps}(\theta_A)$ found by equation (4-5) delivers the maximum plantar flexor torque at $(\theta_A, \dot{\theta}_A)$. The applied ankle torque by a subject at a certain state must always remain somewhere between the maximum plantar flexor and maximum dorsiflexor torque this subject can produce at this state. In addition the foot constraints given in relationships(2-12) has to be satisfied, which is in somecases more restrictive than the strength. In case of the foot constraints are more restrictive than the muscles strength, the maximum applicable torque will be saturated at the highest level which satisfies all the foot constraints.

4.4.4. Probability of recovery at a state, $PoR(X_0)$

Values of $T_{Set}(0)$ for a population sample of 553 adults are available at NITE, 2003. Average (SD) for $T_{PF\,Max}(0)$ and $T_{DF\,Max}(0)$ are $-91.65(56.24)N.m$ and $+47.66(14.58)N.m$, respectively. Figure 4-2 shows the distribution of plantar flexion-dorsiflexion strength data. For a given initial state X_0 a computer program solves the balance recovery problem for each subject (i.e. for each $T_{Set}(0)$ data), integrates the results and delivers which portion of them have the possibility of regaining their stability when released from X_0, which is, by definition, $PoR(X_0)$. PoR hence takes values between zero (0%, no one) and one (100%, everyone).

4.4.5. A faster calculation method

Calculation of the probability of recovery from a certain point in the $x - v$ plain includes solving the recovery problem from that point for the population's strength pairs, whether by integration of differential areas in the probability distribution function (PDF) map, which is the derivative of the cumulative probability shown in Figure 4-3, or by strength pairs data we have for a statistical group. In either case, to get a value for the risk from a single posture, the recovery problem must be solved for many strength pairs.

Furthermore, to solve the recovery problem from a certain posture and for a certain PF-DF strength pair, i.e. to find the possibility of regaining the balance from that posture for a certain set of ankle torque limits, many iterations on torque-time functions must be

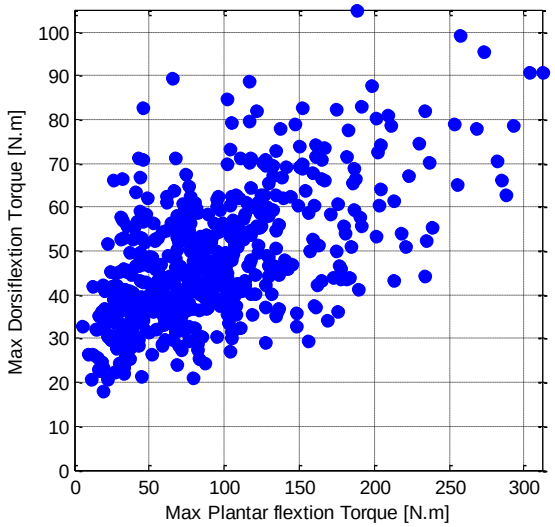

Figure 4-2. Maximum applicable ankle (left) and hip (right) torques at zero angle and velocity condition, for paired lower limbs, for a group of 553 Japanese adults (NITE, 2003). For each subject, data for plantar flexion, dorsiflexion, hip extension, and hip flexion is available.

tested. Thus, to figure out the postural fall initiation risk from a single posture, a great volume of calculations is needed. Finding a risk map for $x - v$ plain will be a very time consuming job.

Fortunately, there is a possibility for dramatically reducing the computational load. Suppose a subject has a maximum isometric voluntary plantar flexor and dorsiflexor torques of $T_{PF\,Max}(0) = 71.52 N.m$ and $T_{DF\,Max}(0) = 32.79 N.m$, respectively. This subject is shown by a star mark in Figure 4-3. It is found that 53% of the population is able to apply torques in both plantar flexion and dorsiflexion directions equal to or greater than those of

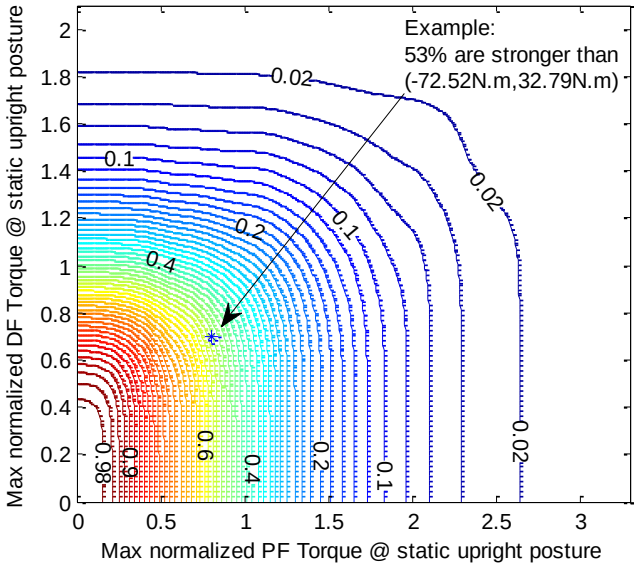

Figure 4-3. Contour map of cumulative probability function based on the statistical data from the NITE (2003). For example it shows 53% of the population are able to apply normalized plantar flexor and dorsiflexor torques of 0.8 and 0.7 (actual torques of -71.52 *N.m* and +32.79 *N.m*), respectively, at a static upright standing posture.

this person. Now, find the balanceable region for this person in the $\bar{x} - \bar{v}$ plane, as introduced in section 3. The balanceable region for this person is the area between the red curve and green curve in Figure 4-4, and this specific subject may regain their balance from all states in this area but will initiate a fall if they start from any other state. Now, one may do the same procedure for other possible subjects, i.e. other PF-DF strength points in Figure 4-2, find the balanceable region for each subject, and by integration of the probability distribution function over the subjects figure out the probability of recovery (PoR) for all states.

For even more simplicity, if we neglect changes of maximum joint torques with ankle angle and angular velocity, the boundaries of the balanceable region which are stable subspaces corresponding to each point on the boundary of the input region, can be found analytically by equation (3-10) as follows

$$X_2{}^2 = -2a\left(\cos(X_1) - \cos(X_{1_0})\right) + 2bu^*\left(X_1(t) - X_{1_0}\right) + X_{2_0}{}^2 \; ; \; X_2(t) \neq 0$$

where u^* is a control input on the boundary of the input region, and

$$X_0 = \begin{bmatrix} \sin^{-1}\left(-\frac{b}{a}u\right) \\ 0 \end{bmatrix} \pm \varepsilon \begin{bmatrix} 1 \\ -\sqrt[4]{a^2 - b^2u^2} \end{bmatrix}$$

and ε is a small scalar, to move X_0 slightly away from the $X_2 = 0$ axis in a true direction.

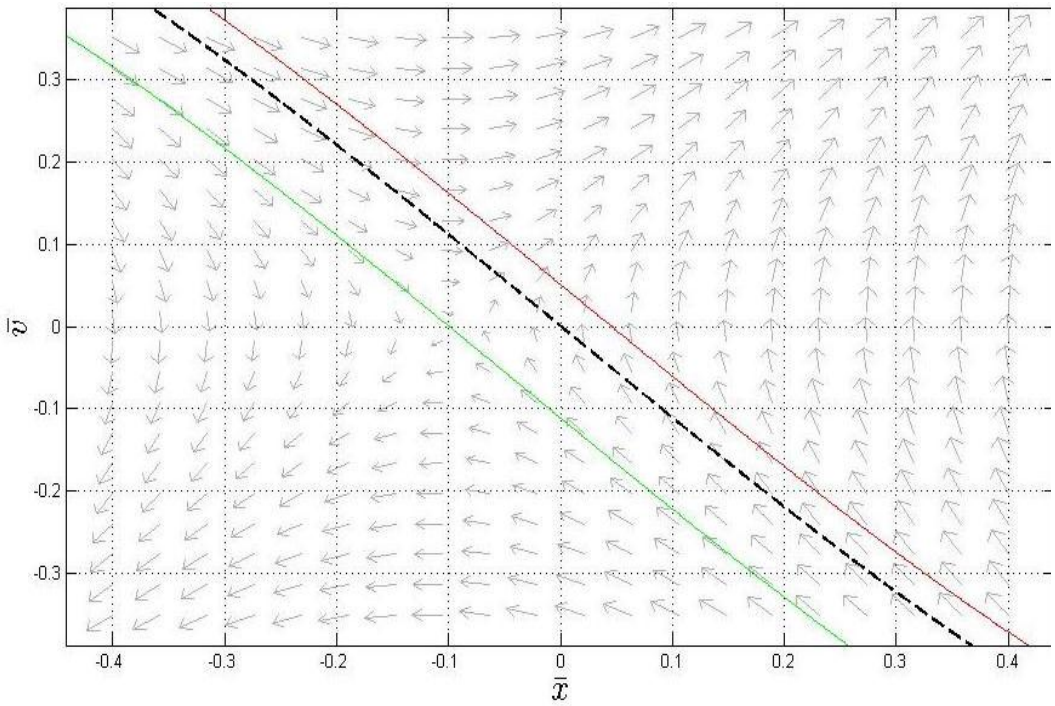

Figure 4-4. Phase plane for maximum plantar flexor torque of a subject with $T_{PF_{Max}} = 71.52N.m$. Green curve is the stable manifold for the maximum plantar flexion torque, and the red curve is the stable manifold for the maximum dorsiflexion torque of $T_{DF_{Max}}(0) = 32.79N.$ The balanceable region for this subject is the area between green and red curves.

By solving the stable subspace for $u^* = T_{PF_{Max}}(0)$ for a subject, this curve will be the contour of the PoR-map with a PoR equal to the portion of the population with a maximum plantar flexion strength ($T_{PF_{Max}}(0)$) equal to or greater than that of this person.

4.5. Results

4.5.1. 2-link model

For a 2-segment mechanical model of section 2.2 and anthropometric parameters of Table 3-1 a MATLAB® program solved PoR for the entire $\hat{x} - \hat{v}$ plane. Satisfaction of foot constraints is guaranteed and when necessary, saturated input is applied. The result is shown in Figure 4-5. The model is facing to the left, and the positive direction implies posterior movement. The dark red color means nobody will lose their balance, and dark blue means everybody will lose their balance. This figure shows that recovery is not possible except in a diagonal feasible region, the boundaries of which are imposed by foot constraints: keeping the CoP between heels and toes (lateral boundaries) and keeping the GRF upward (both ends). The origin corresponds to the CoM exactly above the ankle without moving, and is colored as dark red. States around the origin and those spreading along a particular diagonal curve, corresponding to those inclined postures having a proper returning velocity are the safest states.

As a general trend, stability reduces with distance to the safe curve. It happens

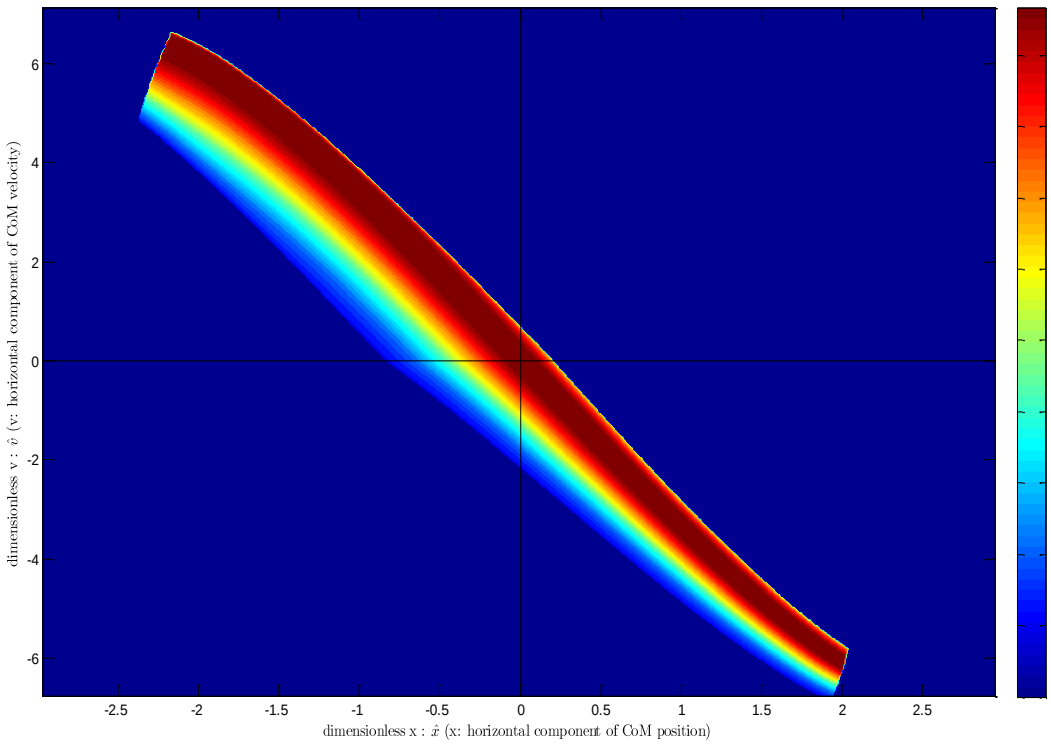

Figure 4-5. Color-map of the probability of recovery (PoR) for the 2-link model of section 2.2, in $\hat{x} - \hat{v}$ plane. Red means high PoR (1) and blue means low PoR (0). Recovery may be possible only in a diagonal feasible region. The subject is facing to the left and positive $\hat{x}$ means backward inclination. Origin of the coordinate system ($\hat{x} = \hat{v} = 0$) implies the static upright posture.

gradually on the left side (anterior displacement of the CoM) while a sudden drop to zero takes place on the right side (posterior displacement). The reason is simple: in the posterior movement of the CoM, the CoP arrives to its final location (the heel) very soon, beyond which there is no possibility to recover without stepping backward. While in anterior movements, CoP can move longer, and thus, the strength of joints is the key in most cases.

4.5.2. 3-link model

For the 3-segment model of section 2.3 PoR may be calculated for every single point in the 4-dimensional state space ($X = \left[\theta_L, \theta_H, \dot{\theta}_L, \dot{\theta}_H\right] \in \mathbb{R}^4$). Here it is shown for states on a 2-dimensional subspace of equal legs and HAT angles, and equal velocities, i.e.

$$\theta_L = \theta_H \;\&\; \dot{\theta}_L = \dot{\theta}_H \;\; at\; t = 0 \qquad (4\text{-}7)$$

mapped on the $\hat{x} - \hat{v}$ plane, the axes of which are the horizontal displacement of CoM of the entire body (except feet) normalized to the foot length ($\hat{x}$), and its time derivative ($\hat{v}$):

$$\begin{aligned} \hat{x} &= -\frac{l_{L_{CM}} \sin(\theta_L) m_L + \left(l_{L_H} \sin(\theta_L) + l_{H_{CM}} \sin(\theta_H)\right) m_H}{l_F (m_L + m_H)} \\ \hat{v} &= -\frac{l_{L_{CM}} \cos(\theta_L) \dot{\theta}_L m_L + \left(l_{L_H} \cos(\theta_L) \dot{\theta}_L + l_{H_{CM}} \cos(\theta_H) \dot{\theta}_H\right) m_H}{l_F (m_L + m_H)} \end{aligned} \qquad (4\text{-}8)$$

During the recovery states may go out of this plane by hip flexion/extension.

A MATLAB® program solved the PoR for about 1000 initial states intelligently scattered on the $\hat{x} - \hat{v}$ plane. Average anthropometric parameters (Winter, 2009, see Table 3-2) were used. Satisfaction of foot constraints is guaranteed and when necessary, saturated input is applied. The result is then interpolated for the entire plane (PoR-map) and shown in Figure 4-6.

4.5.3. Risk of loss of balance on a train

Risk of loss of balance is the complimentary of the probability of recovery (1 minus PoR). In order to present a practical example, risk of loss of balance for a person standing on a train will be considered in this section.

For the same 2-link model of section 4.5.1, Figure 4-7 shows a color-map of postural risk of loss of balance at any posture within the range of motion of the ankle joint, obtained by the fast calculation method and with consideration of changes of the maximum voluntary ankle torque with ankle angle and angular velocity. In this figure, the dark red color means no one is able to regain stability under the assumptions of this paper (high risk) and dark blue means everyone may regain their balance (no risk). The black dashed curve is the no-risk curve. The ankle range of motion is supposed to be -0.7rad~+0.5rad (as stated in section 2.2), which corresponds to the range of $\bar{x}$ as -0.48~+0.64. For the most dorsiflexed case ($\bar{x} = -0.48$) the maximum possible range of $\bar{v}$ was found to be +0.275~+0.512, while 50% of people cannot control their balance for velocities less than +0.355. The upper bound is the same (0.512). The maximum tolerable plantar flexed situation was found to be $\bar{x} = -0.540$ for which a forward velocity of $\bar{v} = -0.492$ is

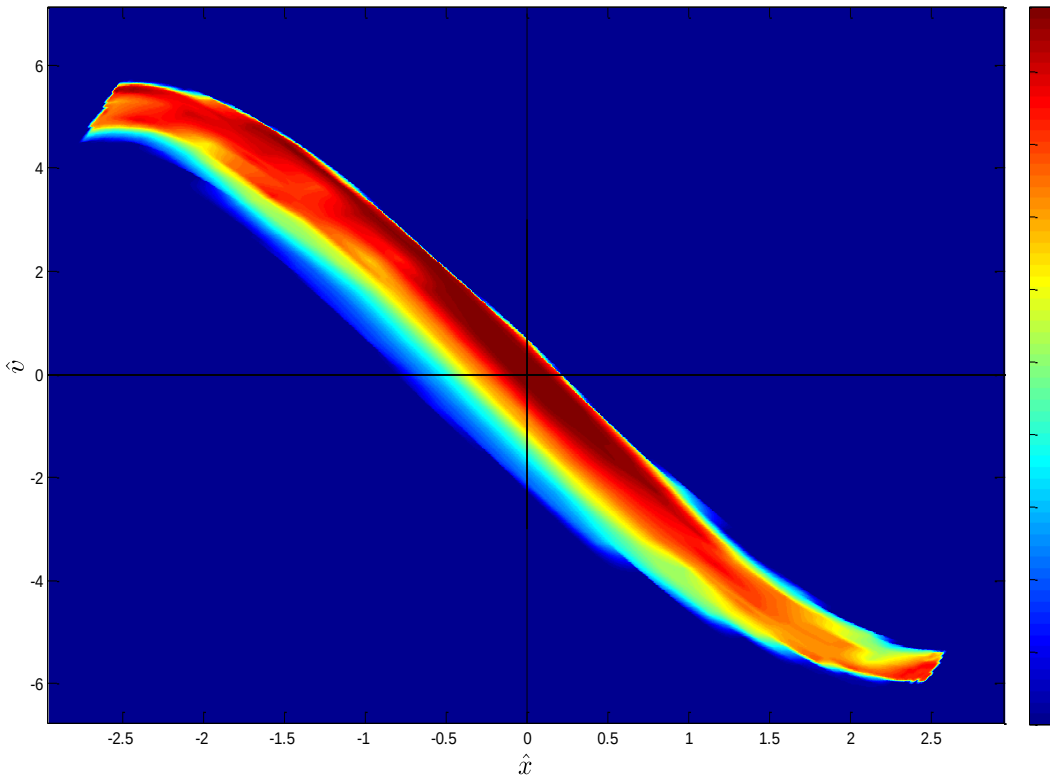

Figure 4-6. Color-map of the probability of recovery (PoR) for the 3-link model of section 2.3, in $\hat{x} - \hat{v}$ plane. Red (1) means high PoR which implies low-risk of fall initiation, blue (0) means no possibility to recover unless taking a step(s). Thus, recovery may be possible only in a diagonal feasible region. The subject is facing to the left, thus, positive $\hat{x}$ means backward inclination. Origin of the coordinate system ($\hat{x} = \hat{v} = 0$) implies the situation in which the center of mass of the body is exactly above the ankle and doesn't move, i.e. static upright posture.

necessary to make recovery possible for some subjects. The maximum tolerable forward normalized velocity is -0.581 (@ $\bar{x} = -0.512$). For static postures ($\bar{v} = 0$), the possible range of $\bar{x}$ is $-0.214 \sim +0.050$ which is exactly – as expected – the foot length. However, 50% of people are not able to keep their balance outside the area of $\bar{x} = -0.113 \sim +0.050$.

Risk of loss of balance for a person standing on a train for several conditions is given in Table 4-2. The person is in a erect stance situation when the train sudenly brakes with a deceleretion of a. A forward perturbation means the person is facing toward the head of the train, and a backward perturbation means they are facing to the rear. Delay time, t_D, is the delay between perturbation onset and recovery start. The initial situation for the recovery trial is given by $(\bar{x}, \bar{v})$. All initial states given in this table are shown in Figure 4-7. The last row for each t_D shows the lowest accelereation with 100% risk, which in some cases are higher than what happens in a train in practice. It shows, for example, 98% of those with a relatively fast response (75*ms*) are able to control their balance under a sudden backward braking deceleration of *0.1g*, which is quite normal in daily transportation, while a response delay of 150*ms* makes stepping unavoidable. In forward perturbation the risk of loss of balance for a *0.26g* deceleration, which might happen in

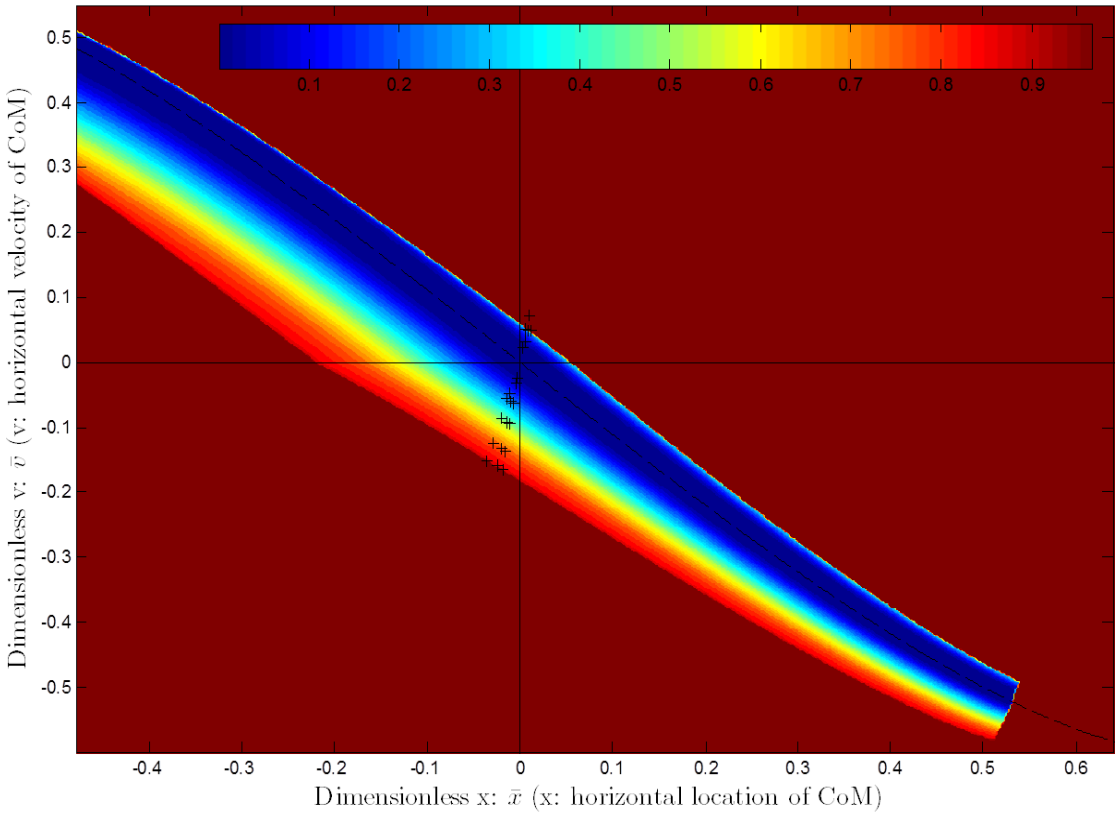

Figure 4-7. Color-map of the risk of loss of balance. Red (1) means high risk, blue (0) means no risk. $\bar{\boldsymbol{x}}$ range is set to $[-0.48, +0.64]$ to keep the ankle angle within its range of motion. The subject is facing to the left, thus, positive $\bar{\boldsymbol{x}}$ means backward inclination. Origin of the coordinate system ($\bar{\boldsymbol{x}} = \bar{\boldsymbol{v}} = \mathbf{0}$) implies the situation in which center of mass of the body is exactly above the ankle and doesn't move, i.e. a static upright posture. Black dashed curve is the no-risk curve (NRC). Small black plus marks: initial states for recovery trial after forward/backward deceleration perturbation on a train, for conditions stated in Table 4-2.

Table 4-2. Risk of loss of balance for a person standing on a train when the train suddenly brakes with a deceleration of a. Forward perturbation means the person is facing toward the head of the train. Delay time, t_D, is the delay between perturbation onset and recovery start. Initial situation for the recovery trial is given by $(\bar{x}, \bar{v})$

t_D [ms]	75			100			150		
	$\boldsymbol{a}$ $[\boldsymbol{m/s^2}]$	$\bar{\boldsymbol{x}}$ $\bar{\boldsymbol{v}}$	***Risk***	$\boldsymbol{a}$ $[\boldsymbol{m/s^2}]$	$\bar{\boldsymbol{x}}$ $\bar{\boldsymbol{v}}$	***Risk***	$\boldsymbol{a}$ $[\boldsymbol{m/s^2}]$	$\bar{\boldsymbol{x}}$ $\bar{\boldsymbol{v}}$	***Risk***
Forward Perturbation	1.0	-0.003 -0.024	4%	1.0	-0.005 -0.032	7%	1.0	-0.011 -0.048	20%
	2.6	-0.007 -0.062	25%	1.9	-0.010 -0.061	25%	1.2	-0.014 -0.057	25%
	4.0	-0.011 -0.095	50%	2.9	-0.015 -0.092	50%	1.8	-0.020 -0.086	50%
	5.8	-0.016 -0.138	75%	4.2	-0.021 -0.134	75%	2.6	-0.029 -0.124	75%
	6.9	-0.019 -0.165	100%	5.0	-0.025 -0.159	100%	3.2	-0.036 -0.153	100%
Backward Perturbation	1.0	0.003 0.024	2%	1.0	0.005 0.032	5%	1.0	0.011 0.048	100%
	2.1	0.006 0.050	100%	1.5	0.008 0.048	100%	0.94	0.0106 0.072	100%

emergency braking, will be 25%, 43%, and 75%, after 75*ms*, 100*ms*, and 150*ms* of response delay, respectively. One may use the method introduced in this study to consider the stability of states in other actions and tests, such as walking, sit-to-stand, stepping threshold tests, etc. For example, in walking, after a heel strike, when the other limb bears almost no portion of the body weight, the position and velocity of the CoM may be used to figure out the risk of loss of balance. In such a case it should be noted that the strength of only one limb should be accounted for.

4.6. Discussion

A new measure for postural upright stability was introduced in this section to describe quantitatively how good the balance is in a certain situation (state), which assigns a value to a body state based on the probability of successfully maintaining the balance. PoR calculated on a 3-link and a 2-link dynamic model is shown for all states in a 2-dimentsional space mapped in the $\hat{x} - \hat{v}$ plane. In the followings, PoR will be compared to the conventional stability measure: MoS, PoR obtained by the 3LM will be compared to that of 2LM, and limitations of this work will be discussed.

4.6.1. PoR vs MoS

MoS as defined by Hof et al. (2005) is

$$MoS = \begin{cases} l_F - XcoM & ; XcoM \geq l_F/2 \\ XcoM & ; XcoM < l_F/2 \end{cases}$$

where $XcoM = x + v/\omega_0,\ \omega_0 = \sqrt{g/l_{B_{cm}}},\ x = x_A - l_{B_{cm}}\sin\theta_B,\ v = dx/dt$. Positive MoS implies the feasible recovery. It is normalized and shown for the $\hat{x} - \hat{v}$ plane in Figure 4-8(a). Black lines are the MoS contours of 0.50 and 0.00. The same contours of PoR for the 2LM and 3LM are included for comparison as green and blue curves, respectively. MoS takes one on a line ($\hat{v} = -\omega_0\hat{x} - \omega_0(2x_A - l_F)/2l_F$), and linearly reduces with distance from this line, while the distribution pattern for PoR is quite different.

MoS may be very small for a state while it is highly safe: at $[\hat{x} \quad \hat{v}] = [0.16 \quad 0]$ MoS is 0.05 while PoR is 0.90 (Figure 4-8(b)). Or at $[\hat{x} \quad \hat{v}] = [0 \quad 0.51]$ MoS=0.07 versus PoR=0.90 (Figure 4-8(c)). The reverse is also true: high MoS doesn't necessarily mean that recovery is easy for everybody. At $[\hat{x} \quad \hat{v}] = [-0.31 \quad 0]$ where according to MoS the stability is maximum, only 70% of the population is able to control their balance. The required plantar flexor torque at this posture is not applicable by the others. Also, for points out of the feasible region nobody may recover their balance without taking a step, which is not possible in the mechanical model of this study as well as that of MoS. Thus PoR=0 constantly, while MoS keeps reducing, e.g. from -0.40 at p3 to -0.86 at p4.

Furthermore, in an erect standing position small excursions of the vertical projection of the CoM around the ankle are pretty safe and should not affect an upright stability index as much as those near the toe or heel. This is exactly what can be seen on the PoR-map: the maximum value with a small gradient on and around the origin, while MoS largely varies with the state, e.g. from p1 to p2 in Figure 4-8(a) and (b) PoR changes from 1.00 to 0.90

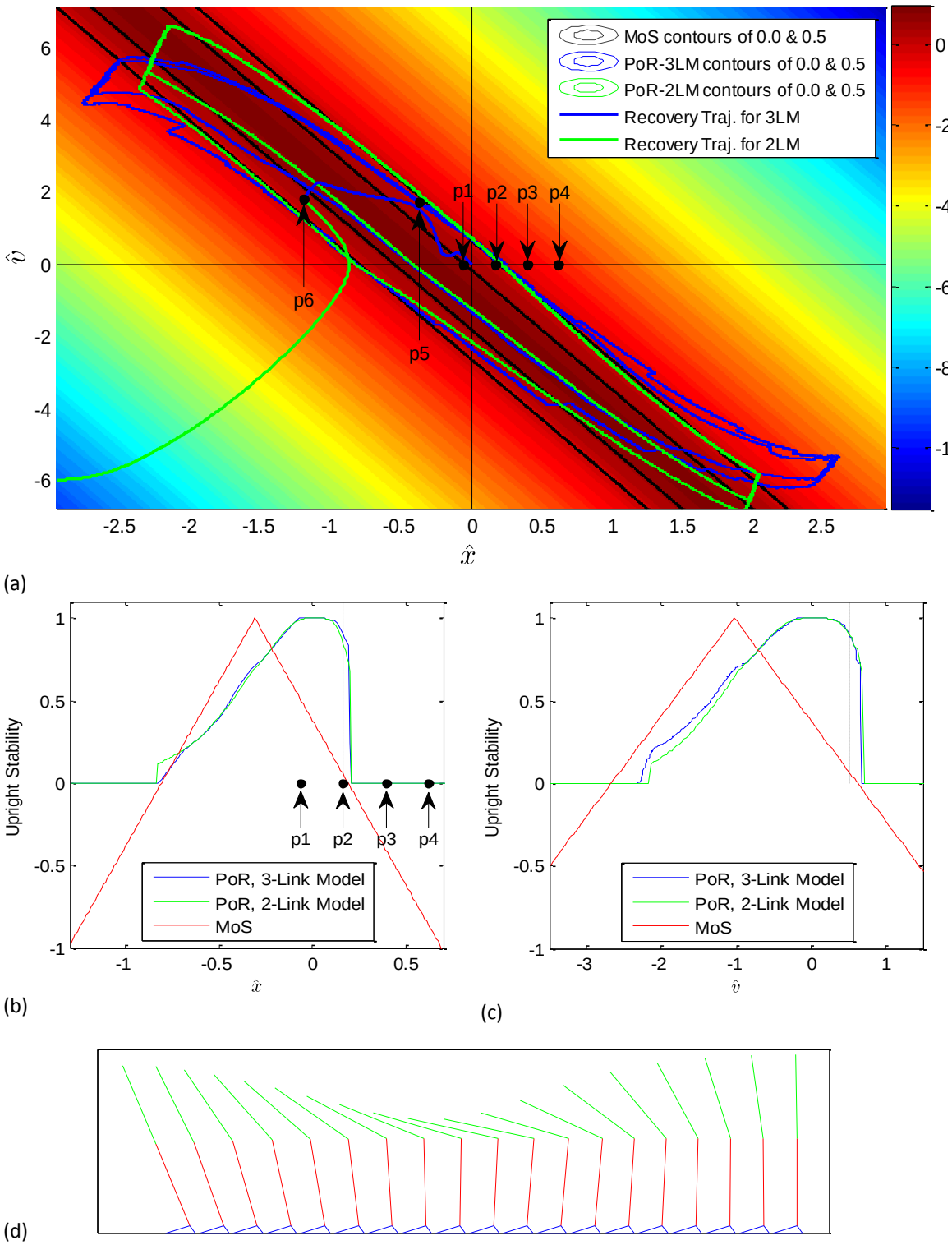

Figure 4-8. (a) Margin of stability (MoS) for the $\hat{x} - \hat{v}$ plane, normalized to its maximum. Dark red corresponds to 1 (highest stability). Black curves are contours of 0 and 0.50 of MoS. The inner curve corresponds to 0.50. Green and blue curves are contours of 0 and 0.50 (inner) of the probability of recovery (PoR) for the 2-link model and 3-link model, respectively. Part of the 0.50 contours overlap with the 0 contours. The thick blue curve shows the recovery trajectory of the 3-link model from p6. The thick green curve shows the best attempt of the 2-link model from the same point. (b) A cross section of PoR-2LM, PoR-3LM, and MoR at $\hat{v} = 0$, and (c) at $\hat{x} = 0$. Points p1~p4 are equally distanced. (d) A stick view of the recovery trajectory from p5 by the 3-link model for 50ms intervals.

while MoS drops from 0.50 to 0.05. The sensitivity of PoR to $(\hat{x}, \hat{v})$ has its maximum on the boundary of the feasible region, while MoS has a uniform gradient everywhere.

In fact, the physical interpretation of MoS is the minimum momentum which brings the subject to the edge of a loss of balance. Following a perturbation onset and at the initial state of the recovery trial, when there is no external intervention, it is PoR that addresses how likely it is to lead to a loss of balance, and hence, describes how good the balance is in the situation.

4.6.2. 2-Link Model vs 3-Link Model

Dynamics of the 2-link model (2LM) and 3-link model (3LM) are not so different in configurations determined by condition (4-7) since the third link's length ($l_{H_{CM}}$) is small. Thus, $PoR(\hat{x}, \hat{v})$ in Figures 4-5 and 4-6, as well as its contours and cross sections in Figure 4-8 show a similar pattern in general. Minor differences mainly come from 1) Hip bending which makes the 3LM more capable in momentum management. See how a 3-link modeled individual $[T_{PF\,max}, T_{DF\,max}, T_{HE\,max}, T_{HF\,max}] = [-120, +50, -120, +250]$ recovers from a forward-inclined state with a backward velocity smaller than what is necessary for an easy recovery (p5: $[\hat{x} \quad \hat{v}] = [-1.2 \quad +1.8]$). The hip starts with a flexor torque in order to speed up backward movement of Legs, and then quickly turns to an extensor torque. The stick view (50ms intervals) and state trajectory of such a movement is shown in Figure 4-8(d) and (a), respectively. This individual, if modeled as a 2LM, cannot recover from p5. The state trajectory of its best 2LM attempt is shown in Figure 4-8(a) as well. PoR at p5 by 3LM and 2LM is 30.03% and 23.77%, respectively. 2) The torque limit on the hip joint of the 3LM prevents the application of torques big enough in some states. Thus, for example, at p6 ($[\hat{x} \quad \hat{v}] = [-0.38 \quad +1.7]$) PoR declared by the 3LM (58%) is less than that of the 2LM (98.24%).

Anomalies in the PoR distribution pattern for the 3LM should be mainly related to the simplifications and inaccuracies associated with the nature of this study's numerical solution algorithm, since the computational burden was much heavier in this case than that in the 2LM.

However, the story is different for initial states other than those of condition (4-7) where PoR by the 2LM (as well as MoS) might be far wrong, because of the lack of ability of a 2LM to simulate a 3LM dynamics. As an example, consider an upright standing posture with the velocity of Legs and HAT parts in an opposite direction but a zero velocity of the total CoM. Both PoR by the 2LM and MoS declare this situation highly stable, while there exist velocities for which the situation is not recoverable at all. A 2LM is capable to describe body dynamics only in nearly standing postures, where the distance of the CoM to the BoS remains almost constant and the horizontal excursions of CoM is small regarding the body height.

4.6.3. Foot constraint versus torque limitations

Figure 4-7 says that, except in a diagonal band including the origin, regaining stability, regardless of how strong an individual is, will not be possible under the assumptions of this

paper, e.g., conditions in which no step is to be taken and no support is available other than that from the ground. In that band, the possibility of recovery depends on one's strength.

If we don't care about the ankles' range of motion, the possible region for regaining stability is bounded by four boundaries: two lateral boundaries are imposed by the limitation of the position of the center of pressure, and the other two (northwest and southeast) imposed by the nature of the ground reaction force. These boundaries are shown in Figure 4-9 by solid black lines . Also a map of the postural risk of loss of balance without caring about any constraint, i.e. range of motion and foot constraints (2-11), and without taking into account the variability of the maximum applicable torque with angle and angular velocity (equations 4-5 and 4-6), is shown by a colormap in the same figure. It is interesting to note that the left and right lateral boundaries are the plantar flexion extreme curve (PEC, which is the stable subspace with the maximum applicable plantar flexion torque) with a fall initiation risk of 0.88 (i.e. PoR of 0.12) and dorsiflexion extreme curve (DEC, the stable subspace with the maximum applicable dorsiflexion torque) with a 0.32 risk (PoR=0.68), i.e. when moving from negative $\bar{x}$ to positive, from left to the right in Figure 4-7, at first the risk equals 1, then when the left border is reached it jumps from 1 (dark red) to 0.88 (red), decreases gradually –not uniformly – to zero (dark blue) at the no-risk curve, increases gradually to 0.32 (cyan) at the right border and jumps suddenly to 1 again. It means that for a large majority of the population (88%) in forward bending, the ankle strength matters and defines their possibility of balance control. For the other 12%

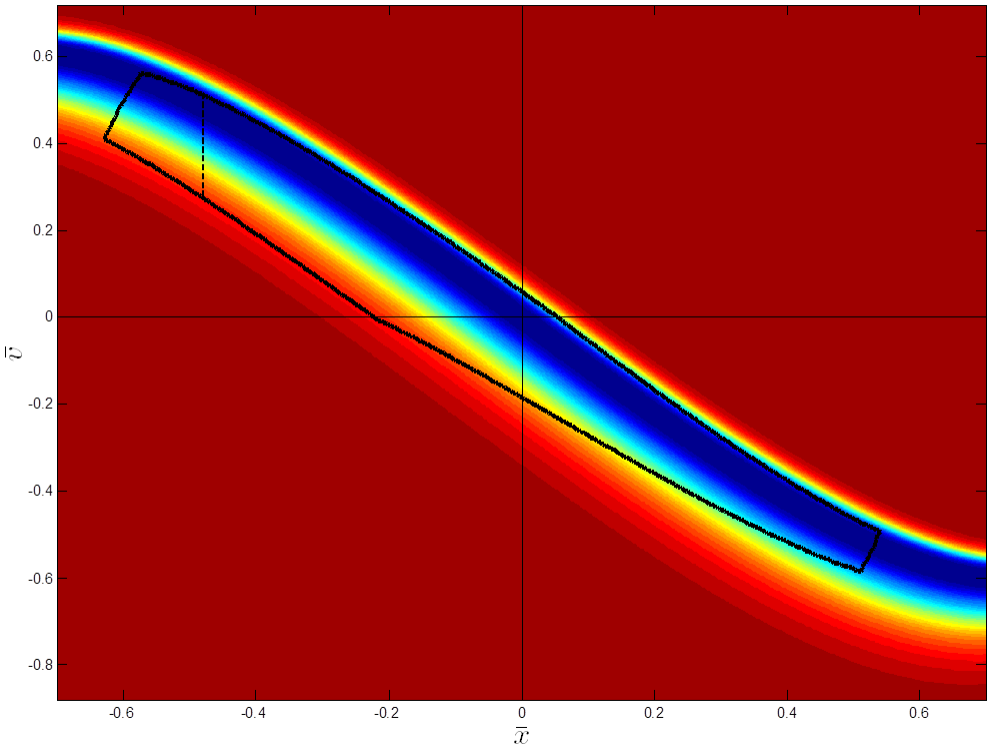

Figure 4-9. Postural risk of fall initiation, without using the torque-angle-velocity relationships. No constraints are applied. Black solid lines indicate the area of possible stability from Figure 4-7. Black dashed line shows the forward bending limit based on the ankle range of motion. Backward bending limit lies at $\bar{x} = 0.643$.

(top strongest subjects), keeping the position of CoP within the supporting area is more restrictive, and therefore, in extreme forward bending postures they cannot use their maximum power. The story for the right lateral boundary is different. The DEC of a 0.32 risk, implies that in backward leaning, the lack of support is dominant, since 68% of the population cannot apply their maximum dorsiflexor torque in extreme backward inclination cases. The reason is, roughly, that the supporting area is extended toward the front side more than to the back, thus, the constraint on the position of the CoP is less restrictive in forward leaning than in backward.

4.6.4. Effect of torque-angle-velocity relations

Human joint torque depends on angle and angular velocity. We included this fact in our solution by using a model for torque-angle-velocity (equations 4-5 and 4-6) to determine the ankle torque at a moment during solving the equation of state (2-6-2). Figure 4-1 showed a negligible difference in no-risk curves found with and without noting this fact. We obtained the risk for the entire $x - v$ plane again ignoring this fact in the solution method, by using equations (3-9) and (3-10). The result, without any constraint, is demonstrated in Figure 4-9. Comparing it to Figure 4-7 suggests that, even though the obtained NRC was almost the same with and without this simplifying assumption, the difference for the entire risk map is noticeable. One difference is that all iso-risk curves are almost parallel in Figure 4-9 while they tend to converge when getting far from the origin in both PF and DF directions, in Figure 4-7. This is mainly because in higher angles – in both directions – one's maximum applicable torque decreases, therefore one can tolerate velocities in a smaller range and closer to that on the NRC. Another difference is that the possible band has rotated slightly counter clockwise in Figure 4-7 with respect to Figure 4-9. The point here is the role of passive torque, which is always concentric. At a backward leaning posture a proper range of forward velocities is tolerable. If we don't ignore the passive torque, which acts in forward direction and collaborates with the forward velocity, a smaller velocity works like a bigger one when passive torque was ignored. Thus, the tolerable velocity range with presence of angle-dependent passive torques has a smaller absolute. In order to ease comparison, the possible stability area of Figure 4-7 is indicated in Figure 4-9 by solid black lines.

4.6.5. Limitations

In order to find a unique solid stability value for a body state, the focus of this work is limited to mechanical characteristics since they may be easily modeled and measured. The role of control skills is put out of view by assuming the controller to work optimally. Therefore, whether a person is physically able to recover or not is the issue, where the maximum torque an individual can apply on his or her joints plays a key role. Inclusion of control/cognitive impairments would be possible by adding a control system model and using statistical probability distribution functions for its parameters.

In this research a 3-link mechanical model was used to introduce and solve PoR which does not include all the joints that play a noticeable role in the control of balance, such as knees and shoulders. PoR estimated based on such a model is not perfect in some states or

$\hat{x}, \hat{v}$ pairs, since it may lose some possible recoveries. One may use the same method on a more complete model in order to find more accurate results, or include medio-lateral movements as well, though the computational time increases with the model complexity. However, taking a step in order to recover one's balance is a different story and is totally put out of view in this study. In order to solve the recovery problem on a biped model a multi-goal trajectory finding problem on a state-variant (or hybrid) dynamic system must be solved, which is computationally very heavy. Nevertheless there are hopes that some analytical methods may be developed to replace some huge parts of the numerical computation.

4.7. Summary

The control of balance is a primary objective in most human movements. In many cases, research or practice, it is essential to quantitatively know how good the balance is at a body posture or at every moment during a task. In this section we suggested a new measure for postural upright stability which assigns a value to a body state based on the probability of avoiding a fall initiation from that state. The balance recovery problem is solved for a population sample using a strength database, and the probability of successfully maintaining the balance is found over the population and called the probability of recovery (PoR). It, therefore, describes an attribute of a body state: how possible the control of balance is, or how safe being at that state is. We also showed the PoR calculated for a 2-link body model and for a 3-link body one for all states on a plane, compare the results, and compare it to a conventional metric: the margin of stability (MoS). It is shown, for example, that MoS may be very low at a state from which most of the people will be able to easily control their balance.

Chapter 5
Conclusion and Suggestions

5.1. Conclusion

In this research we addressed two key questions in the field of human posture control and balance: what condition is to be fulfilled for balance to be maintained, and how good the balance is at a certain body situation.

The condition for the balance to be maintained is interpreted to the question of what is the feasible range of movements for a body to keep its upright balance. A feasible range of movements has been figured out for a two segment mechanical model in its center of mass position – velocity plane, previously. This research shows that for a certain individual with given anatomical and mechanical characteristics, the feasible movements of the CoM, or more generally the range of states at which the control of balance would be possible (the balanceable region), can be analytically found through a mechanical reasoning. A new method to figure out the balanceable region is developed, which, in contrast with the conventional methods, obtains the borders of balanceable region analytically, and hence, it is free from iterative numerical calculations. Thus, this method is computationally lighter than the conventional approaches and the solution, therefore, is very fast. As a result, a thorough parametric study on one's ability to handle balance perturbations comes more practical and may be performed efficiently. One may easily alter the model parameters and follow up how the feasible range of movements will be changed, and hence, the role or effect of each every physical parameter can be studied.

In order to illustrate how the method can be used in practice, the feasible region for a well-known two-segment mechanical model as well as for a more complex three-segment one is found using this approach, and is compared to that found by the conventional method.

The feasible range of body movements for the control of balance that found by this method depends on the physical properties of a body including anatomical parameters as well as the joints' strength and whatever constrains the control input into the model (input constraint). The method suggested in this research works with any arbitrary shape of the input constraint.

In addition, in this research a new metric to assess the postural upright stability has been introduced in order to describe quantitatively how good the balance is in a certain situation (body state). The control of balance is a primary objective in most human movements, and in many cases of fundamental or clinical research, or in practice, it is essential to quantitatively know how good the balance is at a body posture or at every moment during a task.

The key idea behind our proposal of this new metric is that a bigger stability value should be granted to the state from which a smaller portion of the society will not be able

to control their balance. There are some body states from which most of the people can maintain their balance, and some others from which most of the people cannot, and will lose their balance. At the former states the balance is good, and at the later one it is poor. This principle should be addressed in suggestion of the upright stability metric.

The balance recovery problem is solved for a population sample using a strength database, and the probability of successfully maintaining the balance is found over the population and called the probability of recovery (PoR). It, therefore, describes an attribute of a body state: how possible the control of balance is, or how safe being at that state is.

Furthermore, a faster calculation approach is also introduced to replace the time-consuming method of solving the recovery problem for so many times. This approach is based on the analytic solution of the balanceable region.

PoR calculated on a 2-link and a 3-link dynamic model is shown for all states in a 2-dimentsional space mapped in the center of mass position – velocity plane, and it is compared to the conventional stability measure: MoS. It is shown, for example, that MoS may be very low at a state from which most of the people will be able to easily control their balance, and reversely, at a state with the highest MoS still a noticeable portion of the population (e.g. one third) are not able to control their balance and will initiate a fall undoubtedly. PoR, hence, better represents how good the balance is at a given body state, and may be replace the MoS in many studies and clinical researches dealing with upright balance, one's ability to control the balance, and how to improve it.

The PoR as defined in this work shows how probable avoiding a fall initiation is at a body state, but not exactly the actual probability of not falling since many fall initiations may be controlled by taking steps. PoR compares the states directly on the basis of the success of the primitive balance control strategies, and hence, is capable of representing the stability at a body state by a single scalar quantifying how good the balance is, or its complementary, how likely the loss of balance is. A corollary, for example, is that a perturbation, no matter what type or how complicated it is, may be transferred to the state space and replaced with a single scalar: PoR, as a function of the response delay.

5.2. Suggestions for future extensions

Indeed a first idea for extension of such an initial research with simplified mechanical models is to extend the model complexities in order to better simulate a human behavior in the reality. The model in this researh was limited to non-stepping models and to those with sagittal symmetry assumed, i.e. in limitted to the sagittal plane. In an extension the medial-lateral movements in the frontal plane may be included. In this case the definitions and theory presented in this work must be slightly modified, but the story is generally the same.

Addition of the ability of taking a step to the model is a different story. In order to solve the recovery problem on a biped model a multi-goal trajectory finding problem on a state-variant dynamic system must be solved, which is computationally very heavy. Analytical

methods may be developed to replace with some huge parts of numerical computation, or otherwise development of a particular effective numerical algorithm for this case seems necessary.

In this research we used statistical strength data in order to find the PoR at a state, but for anatomical parameters (body height, mass, foot length, etc.) just average values have been used for all the subjects. An extension to this work is to use statistical data for anatomical parameters in order to improve the accuracy of simulating the probability of recovery for the population sample.

Also, In this research the control of balance was regarded only from the mechanical side. The balanceable region was talking about is the region in the state space at which an individual is *mechanically* able to control its balance. In the reality a response to a balance perturbation is always more or less suboptimal, and a person will lose their balance at some states included in their balanceable region, at which they are mechanically able to control their balance. One very interesting research which can be done based on the foundings of this work is to study the optimality of response (OoR) to a perturbation.

One may obtain the actual balanceable region and/or actual PoR for an individual through experiments. Initial states scattered [intelligently] in the state space should be induced to the subject, and the outcome of the balance recovery effort get recorded. The relationship between the actual and theoretical (mechanical) balanceable region and/or PoR shows the OoR for this subject. Changes of OoR may be studied for a person at different situation in order to figure out the role of physical/mental conditions in OoR, or for example before and after some rehabilitation training.

Furthermore, intrapersonal studies on OoR, as well as analysis of OoR in different body states, may reveal useful facts about the nature of optimality of one's response to a perturbation in their balance.

References

Anderson, D. E., Madigan, M. L., & Nussbaum, M. A. (2007). Maximum voluntary joint torque as a function of joint angle and angular velocity: Model development and application to lower limb. *Journal of Biomechanics*, 40, 3105-3113.

Ashley, M. J., Gryfe, C. I., Annies, A. (1977). A longitudinal study of falls in an elderly population. II. Some circumstances of falling. *Age and Ageing*, 6, 211-220

Atkeson, C. and Stephens, B. (2007). Multiple Balance Strategies from One Optimization Criterion. *The IEEE-RAS International Conference on Humanoid Robots*, Pittsburgh, PA.

Beelen, A., & Sargeant, A. J. (1991). Effect of fatigue on maximal power output at different contraction velocities in humans. *Journal of Applied Physiology,* 71, 2332-2337.

Beers, M. H., & Berkow, R. (Eds). (1999). *The Merck Manual*, (17th ed). Whitehouse Station, NJ: Merck Research Labs.

Borelli, G. A. (1680). *On the movement of animals*. (P. Maquet, Trans.). Berlin: Springer. (Translated work published in 1989).

Centers for Disease Control and Prevention. (2010). *Web-based Injury Statistics Query and Reporting System (WISQARS)*. Available from: http://www.cdc.gov/injury/wisqars/index.html

Chow, J. W., Darling, W. G., Hay, J. G., & Andrews, J. G. (1999). Determining the force–length–velocity relations of the quadriceps muscles: III. A pilot study. *Journal of Applied Biomechanics*, 15, 200–209.

Dyson, G. H. G. (1977). *The Mechanics of Athletics*. New York, NY: Holmes & Meier Publishers.

Farina D., Arendt-Nielsen L., Merletti R., & Graven-Nielsen T. (2004). Effect of experimental muscle pain on motor unit firing rate and conduction velocity. *Journal of Neurophysiology*, 91, 1250–1259.

Gabell A., Simons M. A., & Nayak, U. S. (1985). Falls in the healthy elderly: predisposing causes. *Ergonomics*, 28, 965-975.

Gordon, M. E. (1990). An analysis of the biomechanics and muscular synergies of human standing. Ph.D. dissertation, Stanford University, Stanford, CA.

Geurtsen, J. B., Altena, D., Massen, C. H., & Verduin, M. (1975). A model for the description of the standing man and his dynamic behaviour. *Agressologie*, 17, 63–69.

Helbig, A., Abel, O., & Marquardt, W. (1998). Model predictive control for on-line optimization of semi-batch reactors. *Proceedings of American. Control Conference*, Philadelphia, PA, 1695–1699.

Hemami, H., Barin, K., & Pai, Y. C. (2006). Quantitative Analysis of the Ankle Strategy Under Translational Platform Disturbance. *IEEE Transactions on Neural Systems and Rehabilitation*, 14, 470–480

Herman, M., Gallagher, E., & Scott, V. (2006). *The evolution of seniors' falls prevention in British Columbia.* BC Ministry of Health Services.

Hill, A. V. (1938). The heat of shortening and the dynamic constants of muscle. *Proceedings of the Royal Society of London, Series B, Biological Sciences*, 126, 136-195.

Hof, A. L., Gazendam, M. G. J., & Sinke, W. E. (2005). The criterion for dynamic stability. *Journal of Biomechanics,* 38, 1-8.

Honarvar, M. H., Nakashima, M. (2013). Prediction of postural risk of fall initiation based on a two-variable descriptionof body dynamics: Position and velocity of center of mass. *The Journal of Human Movement Science*. DOI: 10.1016/j.humov.2012.11.009.

Honarvarmahjoobin, M., Tazaki, Y., & Imura, J. I. (2009). State waypoint approach to continuous-time nonlinear optimal control problems. *Asian Journal of Control*, 11, 669-676.

Horak, F. B., & Nashner, L. M. (1986). Central programming of postural movements: adaptation to altered support surface con"gurations. *Journal of Neurophysiology*, 55, 1369-1381.

Human Resources and Skills Development Canada (2010). Retrieved April 28, 2010 from: http://www.hrsdc.gc.ca/eng/publications_resources/research/categories/population_aging_e/madrid/page04.shtml.

Imms, F. J., & Edholm, O.G. (1981). Studies of gait and mobility in the elderly. *Age and Aging*, 10, 147-156.

Iqbal, K., & Pai, Y. C. (2000). Predicted region of stablity for balance recovery: motion at the knee joint can improve termination of forward movement. *Journal of Biomechanics*, 33, 1619-1627.

Kannus, P., Parkkari, J., Koskinen, S., Niemi, S., Palvanen, M., Jarvinen, M., & Vouri, I. (1999). Fall-induced injuries and deaths among older adults. *Journal of American Medical Association* 281, 1895–1899.

Kerk, C. J., Chaffin, D. B., Page, G. B., & Hughes, R. E. (1994). A comprehensive biomechanical model using strength, stability, and COF constraints to predict hand force exertion capability under sagittally symmetric static conditions. *IIE Transactions*, 26, 57-67.

King, M. A., & Yeadon, M. R. (2002). Determining subject-specific torque parameters for use in a torque-driven simulation model of dynamic jumping. *Journal of Applied Biomechanics*, 18, 207–217.

Kuo, A. D. (1995). An optimal control model for analyzing human postural balance. *IEEE Transactions on biomedical Engineering*, 42, 87-101.

Kuo. A. D., & Zajac F. E. (1993). Biomechanical analysis of muscle strength as a limiting factor in standing posture. *Journal of Biomechanics*, 26, 137-150.

Le Goic, M., Lecompte, J., Sandoz, B., Laporte, S., Paul Vidal, P. (2012). The descent phase of falls: neuromuscular and mechanical factors. ISPGR & GMF congress, Trondheim, Norway.

Levine, S., Zajac. F. E., Belzer, M. R., & Zomlefer, M. R. (1983). Ankle controls that produce a maximal vertical jump when others are locked. *IEEE Transactions on Automatic Control*, AC-28, 1008-1016.

Nashner, L. M., & McCollum, G. (1985). The organization of human postural movements: a formal basis and experimental hypothesis. *Behavioral and Brain Sciences*, 8, 135-172.

Nashner, L. M., Shupert, C. L., Horak, F. B., & Black, F. (1989). Organization of posture controls: An analysis of sensory and mechanical constraints. *Progress in Brain Research*, 80, 411-418.

NITE: National Institute of Technology and Evaluation (2003). *Maximum voluntary joint torques*. Retrieved from http://www.tech.nite.go.jp/human/Application/search/srTorque.php

O'Loughlin, J. L., Robitaille, Y., Boivin, J-F., & Suissa, S. (1993). Incidence of and risk factors for falls and injurious falls among the community-dwelling elderly. *American Journal of Epidemiology, 137*, 342-354.

Overstall, P. W, Exton-Smith, A. N., Imms F. J., & Johnson, A. L. (1977). Falls in the elderly related to postural imbalance. *British Medical Journal*, 1, 261-264

Pai, Y. C., & Patton, J. (1997). Center of Mass velocity-position predictions for balance control. *Journal of Biomechanics*, 30, 347-354.

Patla, A., Frank, J., & Winter, D. (1990). Assessment of balance control in the elderly: Major issues. *Physiotherapy Canada*, 42, 89-97.

Pilkar, R. B., Moosbrugger, J. C., Bhatkar, V. V., Schilling, R. J., Storey, C. M., & Robinson, C. J. (2007). A Biomechanical model of human ankle angle changes arising from short peri-threshold anterior translations of platform on which a subject stands. *Conference Proceedings - IEEE Engineering in Medicine and Biology Society*, 4308-4311.

Prudham D., & Evans, J. G. (1981). Factors associated with falls in the elderly: a community study. *Age and Ageing*, 10, 141-146

Public Health Agency of Canada (2005). *Inventory of Fall Prevention Initiatives in Canada – 2005*. Ottawa: Division of Aging and Seniors, Public Health Agency of Canada.

Runge, C. F., Shupert, C. L., Horak, F. B., & Zajac, F. E. (1999). Ankle and hip postural strategies defined by joint torques. *Posture and Gait*, 10, 161-170.

Scott, V., Peck, S., & Kendall, P. (2004). *Prevention of Falls and Injuries Among the Elderly: A Special Report from the Office of the Provincial Health Officer*. Victoria BC: Provincial Health Office, BC Ministry of Health Services.

Shumway-Cook, A., & Woolacott, M.H. (1995). *Motor control: Theory and practical applications*. Baltimore, MD :Williams & Wilkins.

Spendiff, O., Longford, N. T., & Winter, E. M. (2002). Effects of fatigue on the torque-velocity relation in muscle, *British Journal of Sports Medicine*, 36, 431-435.

Tinetti, M. E., Baker, D. I., McAvay, G., Claus, E. B., Garrett, P., Gottschalk, M., Koch, M. L., Trainor, K., & Horwitz, R. I. (1994). A multifactorial intervention to reduce the risk of falling among elderly people living in the community. *New England Journal of Medicine*, 331, 821-827.

Tinetti , M. E., & Speechley, M. (1989). Prevention of falls among the elderly. *New England Journal of Medicine*, *320,* 1055-1059.

Winter, D. A. (1995-a). *ABC of balance during standing and walking*. Waterloo, Canada: Waterloo Biomechanics.

Winter, D. A. (1995-b). Human balance and posture control during walking. *Gait and Posture*, 3, 193–214.

Winter, D. A. (2009). *Biomechanics and motor control of human movement* (4th ed.). Hoboken, NJ: John Wily & sons.

World Health Organization (2002). *1997-1999 World Health Statistics Annual*, World Health Organization 2002.

World Health Organization (2008). *Global Report on Falls Prevention in Older Age*. Geneva: World Health Organization.

Yang, F., Passariello, F., & Pai, Y. C. (2008). Determination of instantaneous stability against backward balance loss: two computational approaches. *Journal of Biomechanics*, 41, 1818–1822.

Yang, J. F., Winter, D. A., & Wells, R. P. (1990). Postural dynamics in the standing human. *Biological Cybernetics*, 62, 309-320.

Acknowledgements

All praise is to the God the lord of the universe, the compassionate, the merciful. I should first express my highest gratitude for his blessing and mercy for making this work to be completed.

I also would like to express my thanks to my supervisor, associate professor Motomu Nakashima of the department of mechanical and control engineering, graduate school of science and engineering, Tokyo institute of technology, for his kind help, guidelines, and support throughout this work, without support of whom this work would barely come into reality. Also I have to thank him, the Tokyo Institute of Technology, and the Japanese ministry of education, culture, sports, science and technology for the financial support of me for this work and enabling me to take part in some very valuable and effective conferences/meetings related to this research.

Also, the lab-mates of the Nakashima's Biomechanics laboratory who raised criticisms, and shared their points/comments with me throughout this research term in order to improve the quality and standards of the study. In particular I appreciate their kind contribution in numerical solving of my heavy computer programs by sharing their processors/cores with us in their free times in order to make an efficient cluster computing possible.

Last but not the least, I have to convey my deep thanks to all my friends here in Tokyo for their friendship and emotional support throughout these years, to my little son and daughter for their cooperation without which completion of this work would come too difficult, and in particular to my wife for her understanding, patience, and support that made me quite able to keep concentrating on my research throughout these years.